Control Engineering Practice 154 (2025) 106154

Contents lists available at ScienceDirect

Control Engineering Practice

journal homepage: www.elsevier.com/locate/conengprac

# Time-optimal multi-point trajectory generation for robotic manipulators with continuous jerk and constant average acceleration

Weiguang Yu [a,b,c,d,*], Daokui Qu [a,b,c,e], Fang Xu [a,b,c,d], Lei Zhang [a,b,d], Fengshan Zou [a,b,d], Zhenjun Du [d]

[a] State Key Laboratory of Robotics, Shenyang Institute of Automation, Chinese Academy of Sciences, Shenyang, 110016, China
[b] Institutes for Robotics and Intelligent Manufacturing, Chinese Academy of Sciences, Shenyang, 110169, China
[c] University of Chinese Academy of Sciences, Beijing, 100049, China
[d] Shenyang SIASUN Robot & Automation Co., Ltd, Shenyang, 110168, China
[e] Yellow River Robot Innovation Institute, Jinan, 250000, China

ARTICLE INFO

*Keywords:*
Robotic manipulator
Multi-point trajectory planning
Time optimal
Continuous jerk
Constant average acceleration

ABSTRACT

To meet the demands of high-speed and high-accuracy applications of robotic manipulators, this paper proposes a time-optimal multi-point trajectory planning method with continuous jerk and constant average acceleration. A piecewise sine jerk model is developed for jerk continuity throughout the entire motion profile. An equivalent transformation of this complex model into the simple trapezoidal velocity model is proposed, effectively reducing the computational complexity and ensuring the reliability of real-time planning. The introduction of a parameter, named the trajectory smoothness coefficient, allows for a convenient trade-off between the priorities of speed and smoothness. The adaptive computation algorithm for peak jerk results in a constant average acceleration along paths of any length, ensuring a consistent level of work efficiency regardless of the density of path control points. Through a comprehensive evaluation of the critical constraints for each potential profile type, the single joint's time-optimal and multiple joints' time-synchronized planning problems are solved with closed-form solutions. Furthermore, by designing a multi-joint multi-point velocity look-ahead strategy, time-optimal multi-point trajectory planning for robotic manipulators is realized. Simulation and experimental results on a manipulator demonstrate the effectiveness of the proposed approach in improving time efficiency.

## 1. Introduction

Trajectory planning plays a pivotal role in the field of robots, with extensive applications across a spectrum of tasks, including automated assembly, painting, palletizing, welding, and material handling (Duque et al., 2019; Moghaddam & Nof, 2016; Trigatti et al., 2018). The accuracy of robotic manipulators is crucial for ensuring the quality of the final product, whereas the operational speed of these robots significantly influences the rate of production. However, an excessively aggressive pursuit of efficiency may lead to noticeable fluctuations in robotic movements, potentially inducing mechanical vibrations that can compromise the precision of the robot's trajectory and ultimately have a negative impact on the overall manufacturing quality. Therefore, achieving a harmonious balance between accuracy and speed is vital for the trajectory planning process to ensure optimal performance. Multi-point (MP) trajectory generation is conducted on a continuous path defined by two or more desired path control points. This process is more complex than point-to-point (PTP) trajectory planning, which is limited to just two path control points, as it entails the management of relationships among multiple trajectory segments. Enhancing the performance of MP trajectories for robots is indeed a challenging task. While trajectory planning in the task space is intuitive, it may encounter singularity problems (Huang et al., 2018), necessitating separate planning for position and orientation. Conversely, planning in the joint space avoids these problems by focusing solely joint motion. Hence, this study concentrates on the MP trajectory planning in the joint space, generating smooth, continuous, and time-optimal motion trajectories in real time while meeting kinematic constraints, further enhancing the dynamic performance of robotic manipulators. Traditional time-optimal trajectory planning methods only take into account the time factor (Bobrow et al., 1985; Pham & Pham, 2018), with discontinuous acceleration, resulting in poor trajectory continuity. This can cause structural vibration within the robot (Chettibi, 2019; Heo et al., 2019), diminishing the accuracy of the robot's trajectory and accelerating wear on the mechanical components (Wang et al., 2019).

* Corresponding author at: University of Chinese Academy of Sciences, Beijing, 100049, China.
*E-mail address:* yuweiguang@siasun.com (W. Yu).

https://doi.org/10.1016/j.conengprac.2024.106154
Received 1 June 2024; Received in revised form 20 October 2024; Accepted 23 October 2024
Available online 5 November 2024

Furthermore, abrupt changes in acceleration contradict the physical laws of the robot's actuator, which is difficult to implement effectively in practical applications (Alpers, 2022). Therefore, to enhance the accuracy of robot motion and reduce vibration, it is essential to generate as smooth a motion trajectory as possible, ensuring at least C2 continuous where the acceleration is continuous, so that the jerk (the derivative of acceleration) is bounded. A bounded jerk profile can suppress vibration and improve the tracking accuracy, which has been widely accepted (Fang et al., 2020; Gasparetto & Zanotto, 2010).

In the literature, trajectory planning methods based on polynomial functions subject to specific constraints are commonly employed to achieve a bounded jerk trajectory. Bazaz and Tondu (1999) integrated cubic spline curves with trapezoidal acceleration profiles to generate time-optimal trajectories that meet kinematic constraints; Su et al. (2018) proposed a time-optimal trajectory planning method based on fifth-order Pythagorean-Hodograph (PH) curves for pick-and-place operations of delta robots. Berscheid and Kroeger (2021) proposed the Ruckig algorithm, capable of generating motion trajectories that fulfill third-order complete target constraints in real-time. While these methods can achieve continuous acceleration and thus maintain bounded jerk, they do not guarantee jerk continuity. Discontinuous jerk can diminish trajectory accuracy to some extent and may also contribute to a reduced lifespan of the actuating mechanisms (Visioli, 2000).

Numerous research methods have been developed to address the issue of continuous jerk trajectory. Some studies utilize higher-order polynomials to generate motion trajectories (Fang et al., 2019b; Fung & Cheng, 2014; Gasparetto & Zanotto, 2007; Xie et al., 2016). Nevertheless, achieving jerk continuity, i.e. C3 continuity, necessitates at least a 7th-order polynomial to describe the trajectory accurately. Polynomials beyond the fourth order typically have no closed-form solutions, often requiring iterative optimization methods for solution derivation. This not only escalates computational complexity but also demands increased memory resources in the controller to enhance numerical calculation precision. Additionally, enhanced approaches have been devised based on traditional methods, such as integrating low-order spline curves with optimization algorithms or incorporating trigonometric functions into trajectory descriptions to simplify the computational complexity of trajectory generation (Nguyen et al., 2008). Lee et al. (2011) devised an offline feed rate scheduling algorithm founded on sine velocity profiles for CNC machine tools, adhering to kinematic constraints; however, jerk discontinuities may occur at the beginning and end of variable speed segments. Lin et al. (1983) used a cubic polynomial and iteratively calculated joint motion trajectories to minimize time. Piazzi and Visioli (2000) utilized interval analysis and cubic spline curves to produce globally minimal jerk joint profiles. Simon and Isik (1993) employed fourth-order trigonometric splines for joint space trajectory interpolation, ensuring continuity of the first three derivatives and permitting desired values for the first three derivative constraints at endpoints. While these methods achieve continuous jerk, incomplete velocity constraints at the desired path control points in MP trajectories can cause joint sub-trajectories to move in the opposite direction of the intended motion, resulting in overshoot and undershoot at these points. This diminishes trajectory accuracy of the robot's end effector and heightens the risk of robot collisions (Wu et al., 2023). Visioli (2000) connected two cubic spline curves with a trigonometric spline to notably reduce overshoot; Biagiotti et al. (2020) employed rectangular and harmonic filters to generate motion trajectories described by trigonometric functions online. However, these methods did not take into account the synchronization issue of multiple joints and were unsuitable for multi-joint trajectory planning. Fang et al. (2019) used the sigma function to establish a jerk model and proposed a time-optimal S-curve planning method. Subsequently, they endeavored to refine planning algorithms based on the conventional trigonometric function model, and proposed a smooth joint trajectory planning method based on a 15-phase sine jerk model (Fang et al., 2020). Both methods achieved full trajectory continuity of jerk and addressed the issue of trajectory synchronization. However, the requirement for initial and final velocities to be zero necessitates frequent stops and starts at each path control point in MP motion, which can drastically reduce the time efficiency of the trajectory. Consequently, these methods are not suitable for MP trajectory planning. Addressing numerous critical issues in MP trajectory planning, Wu et al. (2023) proposed a time-optimal trajectory planning approach based on a piecewise motion profile and a series–parallel analytical strategy. However, the method has limitations. It simplifies the trajectory model for synchronization but overlooks the impact of the current end velocity on the starting velocity of the next segment, potentially increasing the total MP trajectory time. Additionally, the requirement for complete path information beforehand can result in extended planning times, affecting the robot's motion responsiveness, especially with many path control points.

Building upon prior efforts, this study introduces an innovative approach for generating MP trajectories by employing a piecewise sine jerk model to address the high-speed and high-accuracy motion requirements of multi-joint robotic manipulators. Compared with existing trajectory planning methods, this approach offers several distinct advantages. Firstly, an equivalent transformation of the complex piecewise sine jerk model into a simple 3-phase trapezoidal velocity model is proposed. And in the transformation process, the introduction of a parameter, named the trajectory smoothness coefficient, allows for a convenient trade-off between the priorities of speed and smoothness. This not only facilitates time-optimal and time-synchronized trajectory generation with continuous jerk and non-zero initial and final velocities, but also significantly enhances the computational efficiency, ensuring the reliability of real-time planning. Secondly, in traditional trajectory planning algorithms with constant jerk limitation, the level of granularity in path segmentation directly impacts the actuator's acceleration capabilities due to kinematic constraints. To address this issue, the proposed planning algorithm in this paper, decouples the relationship between the number of sub-path segments and the acceleration capacity through adaptive adjustment of the peak jerk, achieving a constant average acceleration for paths of any length. This feature ensures a consistent level of work efficiency regardless of the density of path control points, thereby enhancing the adaptability and performance of the trajectory planning algorithm in diverse operational scenarios. Thirdly, this study introduces a local velocity look-ahead strategy integrated with trajectory synchronization techniques. By utilizing a predefined look-ahead depth, this strategy conducts look-ahead planning and synchronization only for the imminent local trajectory segments. By avoiding reliance on global trajectory computations, the proposed method is capable of efficiently generating continuous and synchronized trajectories for multi-joint robots engaged in MP trajectory tasks, thereby significantly improving the real-time performance of trajectory planning and the response speed of motion commands.

The rest of this paper is organized as follows. Section 2 presents the detailed formulation of the piecewise sine jerk model proposed in this study, along with the pertinent mathematical properties. Section 3 discusses the optimization methodologies for time-optimal and time-synchronized trajectories. Section 4 introduces a velocity look-ahead strategy specifically developed for achieving time-optimal MP trajectory planning of multi-joint robotic manipulators. Section 5 provides simulation and experimental results. Finally, Section 6 concludes the paper and suggests directions for potential future research.

## 2. Trajectory model

The MP trajectory planning for robotic manipulators is designed to generate continuous, smooth, and time-optimal motion trajectories along multiple desired path control points described in the joint space. This study focuses on trajectory planning under robot kinematic constraints, excluding dynamics constraints from the scope. Despite the existence of inter-joint interaction forces in actual manipulator motion,

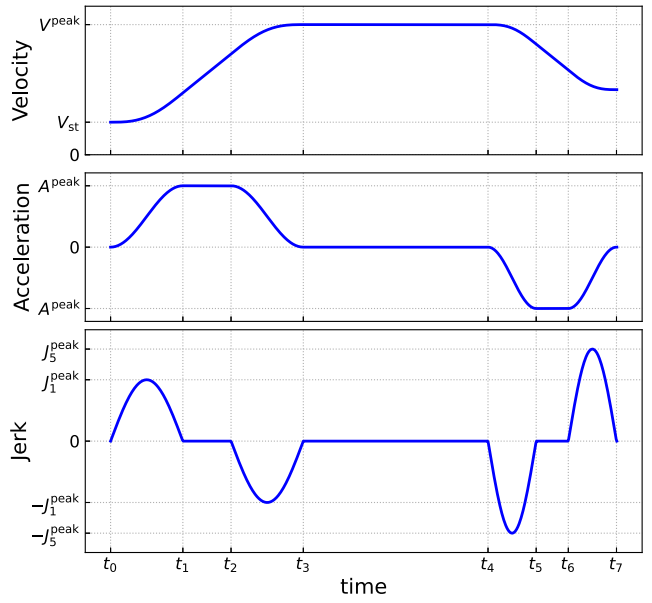


**Fig. 1.** Motion profiles of the proposed 7-phase sine jerk model.

excluding these forces facilitates a more focused study of trajectory generation and optimization, enabling a more direct evaluation of the performance of the method under kinematic constraints. In the absence of consideration for inter-joint interaction forces, the motion of individual joints in the robotic manipulator is typically independent, and the trajectory model remains consistent regardless of the number of joints or the manipulator's configuration. Therefore, this section focuses on the trajectory model for a single joint. In MP trajectories, two adjacent path control points form a sub-trajectory segment, and the entire trajectory is sequentially connected by these sub-trajectory segments. For the sake of convenience in description, this section adopts a single sub-trajectory segment of a single joint as the basic planning unit for the research of the trajectory model. To enhance overall feed speed and minimize total travel time, the trajectory model is designed to maximize the velocities at all intermediate waypoints, with the exception of setting the starting velocity of the first segment and the end velocity of the last segment to zero. In addition, to guarantee continuity and reachability, each sub-trajectory segment is endowed with non-zero constraints for the initial velocity and the maximum final velocity. The flexibility inherent in a manipulator is significant and must not be ignored. For flexible structures, higher-order continuity of the motion trajectory can reduce systematic vibration and improve the accuracy of the motion trajectory. Based on these considerations, the proposed trajectory model aims to ensure the continuity of jerk while achieving the optimal trajectory speed.

### 2.1. Piecewise sine jerk model

The complete piecewise sine jerk model proposed in this paper consists of seven sub-trajectory phases, including four sine jerk phases, two constant acceleration phases, and one constant velocity segment, while ensuring the continuity at the jerk level. Fig. 1 illustrates a graphical representation of the velocity, acceleration, and jerk profiles of this model from top to bottom. Here, $t_i\,(i=0,1,\ldots,7)$ denotes the temporal boundary distinguishing each phase.

The jerk profile is represented as the following unified trigonometric function:

$$j\,(t)=J_i^{\text{peak}}\sin\left(\frac{\pi}{T_i}\tau_i\right),i=1,2,\ldots,7 \tag{1}$$

where $J_i^{\text{peak}}$ is the absolute value of the peak jerk in the $i$th phase, and the jerk of the second, fourth, and sixth phases is always zero, i.e., $J_2^{\text{peak}}=J_4^{\text{peak}}=J_6^{\text{peak}}=0$; $T_i$ is the duration of the $i$th phase, and $T_1=T_3$, $T_5=T_7$; and $\tau_i=t-t_{i-1}$ represents the relative time within the $i$th interval $[t_{i-1},t_i]$ starting from $t_{i-1}$. Combining the above conditions, the jerk profile can be represented by the following piecewise function:

$$j(t)=\begin{cases}J_1^{\text{peak}}\sin\left(\frac{\pi}{T_1}\tau_1\right) & t_0\le t<t_1\\ 0 & t_1\le t<t_2\\ -J_1^{\text{peak}}\sin\left(\frac{\pi}{T_1}\tau_3\right) & t_2\le t<t_3\\ 0 & t_3\le t<t_4\\ -J_5^{\text{peak}}\sin\left(\frac{\pi}{T_5}\tau_5\right) & t_4\le t<t_5\\ 0 & t_5\le t<t_6\\ J_5^{\text{peak}}\sin\left(\frac{\pi}{T_5}\tau_7\right) & t_6\le t<t_7\end{cases} \tag{2}$$

The functions $a(t)$, $v(t)$, $d(t)$ are utilized to denote acceleration, velocity, and displacement, respectively. The symbol $V_{\text{st}}$ represent the initial velocity of the trajectory segment, with the initial displacement and initial acceleration at $t_0$ set to zero, namely,

$$\begin{cases}a(t_0)=0\\ v(t_0)=V_{\text{st}}\\ d(t_0)=0\end{cases} \tag{3}$$

Then, the corresponding acceleration, velocity, and displacement profiles can be obtained by integrating the jerk function with the initial conditions of each phase:

$$\begin{cases}a(t)=a(t_i)+\int_{t_i}^{t}j(t)dt\\ v(t)=v(t_i)+\int_{t_i}^{t}a(t)dt\\ d(t)=d(t_i)+\int_{t_i}^{t}v(t)dt\end{cases} \tag{4}$$

During the first phase, for $t\in[t_0,t_1]$,

$$\begin{cases}a(t)=\frac{J_1^{\text{peak}}T_1}{\pi}\left[1-\cos\left(\frac{\pi}{T_1}\tau_1\right)\right]\\ v(t)=V_{\text{st}}+\frac{J_1^{\text{peak}}T_1}{\pi}\left[\tau_1-\frac{T_1}{\pi}\sin\left(\frac{\pi}{T_1}\tau_1\right)\right]\\ d(t)=V_{\text{st}}\tau_1+\frac{J_1^{\text{peak}}T_1}{2\pi}\tau_1^2+\frac{J_1^{\text{peak}}T_1^3}{\pi^3}\left[\cos\left(\frac{\pi}{T_1}\tau_1\right)-1\right]\end{cases} \tag{5}$$

During the second phase, for $t\in[t_1,t_2]$,

$$\begin{cases}a(t)=\frac{2J_1^{\text{peak}}T_1}{\pi}\\ v(t)=V_{\text{st}}+\frac{J_1^{\text{peak}}T_1}{\pi}[2\tau_2+T_1]\\ d(t)=V_{\text{st}}T_1+\frac{J_1^{\text{peak}}T_1^3}{\pi}\left(\frac{1}{2}-\frac{2}{\pi^2}\right)+\left(V_{\text{st}}+\frac{J_1^{\text{peak}}T_1^2}{\pi}\right)\tau_2+\frac{J_1^{\text{peak}}T_1}{\pi}\tau_2^2\end{cases} \tag{6}$$

During the third phase, for $t\in[t_2,t_3]$,

$$\begin{cases}a(t)=\frac{J_1^{\text{peak}}T_1}{\pi}\left[\cos\left(\frac{\pi}{T_1}\tau_3\right)+1\right]\\ v(t)=V_{\text{st}}+\frac{J_1^{\text{peak}}T_1}{\pi}\left[T_1+2T_2+\tau_3+\frac{T_1}{\pi}\sin\left(\frac{\pi}{T_1}\tau_3\right)\right]\\ d(t)=V_{\text{st}}(T_1+T_2)+\frac{J_1^{\text{peak}}T_1}{\pi}\left[\left(\frac{1}{2}-\frac{1}{\pi^2}\right)T_1^2+T_1T_2+T_2^2\right]\\ +\left[V_{\text{st}}+\frac{J_1^{\text{peak}}T_1}{\pi}(T_1+2T_2)\right]\tau_3+\frac{J_1^{\text{peak}}T_1}{2\pi}\tau_3^2-\frac{J_1^{\text{peak}}T_1^3}{\pi^3}\cos\left(\frac{\pi}{T_1}\tau_3\right)\end{cases} \tag{7}$$

During the fourth phase, for $t\in[t_3,t_4]$,

$$\begin{cases}a(t)=0\\ v(t)=V_{\text{st}}+\frac{2J_1^{\text{peak}}T_1}{\pi}(T_1+T_2)\\ d(t)=V_{\text{st}}(2T_1+T_2)+\frac{J_1^{\text{peak}}T_1}{\pi}(2T_1^2+3T_1T_2+T_2^2)\\ +\left[V_{\text{st}}+\frac{2J_1^{\text{peak}}T_1}{\pi}(T_1+T_2)\right]\tau_4\end{cases} \tag{8}$$

During the fifth phase, for $t \in [t_4, t_5]$,

$$\begin{cases} a(t) = \frac{J_5^{\text{peak}} T_5}{\pi}\left[\cos\left(\frac{\pi}{T_5}\tau_5\right) - 1\right] \\ v(t) = V_{\text{st}} + \frac{2J_1^{\text{peak}} T_1}{\pi}(T_1 + T_2) + \frac{J_5^{\text{peak}} T_5}{\pi}\left[\frac{T_5}{\pi}\sin\left(\frac{\pi}{T_5}\tau_5\right) - \tau_5\right] \\ d(t) = V_{\text{st}}(2T_1 + T_2 + T_4) + \left[V_{\text{st}} + \frac{2J_1^{\text{peak}} T_1}{\pi}(T_1 + T_2)\right]\tau_5 \\ + \frac{J_1^{\text{peak}} T_1}{\pi}(2T_1^2 + 3T_1T_2 + T_2^2 + 2T_1T_4 + 2T_2T_4) \\ - \frac{J_5^{\text{peak}} T_5}{2\pi}\tau_5^2 + \frac{J_5^{\text{peak}} T_5^3}{\pi^3}\left[1 - \cos\left(\frac{\pi}{T_5}\tau_5\right)\right] \end{cases} \tag{9}$$

During the sixth phase, for $t \in [t_5, t_6]$,

$$\begin{cases} a(t) = -\frac{2J_5^{\text{peak}} T_5}{\pi} \\ v(t) = V_{\text{st}} + \frac{2J_1^{\text{peak}} T_1}{\pi}(T_1 + T_2) - \frac{J_5^{\text{peak}} T_5}{\pi}[2\tau_6 + T_5] \\ d(t) = V_{\text{st}}(2T_1 + T_2 + T_4 + T_5) + \frac{J_5^{\text{peak}} T_5^3}{\pi}\left(\frac{2}{\pi^2} - \frac{1}{2}\right) \\ + \frac{J_1^{\text{peak}} T_1}{\pi}(T_1 + T_2)(2T_1 + T_2 + 2T_4 + 2T_5) \\ + \left[V_{\text{st}} + \frac{2J_1^{\text{peak}} T_1}{\pi}(T_1 + T_2) - \frac{J_5^{\text{peak}} T_5^2}{\pi}\right]\tau_6 - \frac{J_5^{\text{peak}} T_5}{\pi}\tau_6^2 \end{cases} \tag{10}$$

During the seventh phase, for $t \in [t_6, t_7]$,

$$\begin{cases} a(t) = -\frac{J_5^{\text{peak}} T_5}{\pi}\left[1 + \cos\left(\frac{\pi}{T_5}\tau_7\right)\right] \\ v(t) = V_{\text{st}} + \frac{2J_1^{\text{peak}} T_1}{\pi}(T_1 + T_2) - \frac{J_5^{\text{peak}} T_5}{\pi}(2T_6 + T_5) \\ - \frac{J_5^{\text{peak}} T_5}{\pi}\left[\tau_7 + \frac{T_5}{\pi}\sin\left(\frac{\pi}{T_5}\tau_7\right)\right] \\ d(t) = V_{\text{st}}(2T_1 + T_2 + T_4 + T_5 + T_6) - \frac{J_5^{\text{peak}} T_5}{2\pi}\tau_7^2 \\ + \frac{J_5^{\text{peak}} T_5}{\pi}\left[\left(\frac{1}{\pi^2} - \frac{1}{2}\right)T_5^2 - T_5T_6 - T_6^2\right] + \frac{J_5^{\text{peak}} T_5^3}{\pi^3}\cos\left(\frac{\pi}{T_5}\tau_7\right) \\ + \frac{J_1^{\text{peak}} T_1}{\pi}(T_1 + T_2)(2T_1 + T_2 + 2T_4 + 2T_5 + 2T_6) \\ + \left[V_{\text{st}} + \frac{2J_1^{\text{peak}} T_1}{\pi}(T_1 + T_2) - \frac{J_5^{\text{peak}} T_5}{\pi}(2T_6 + T_5)\right]\tau_7 \end{cases} \tag{11}$$

Note that the second and sixth phases have constant acceleration, the fourth segment has a constant velocity, and the local peak value of acceleration within the first three phases occurs at $t = t_1$ and is represented by:

$$A_{(1-3)}^{\text{peak}} = \frac{2J_1^{\text{peak}} T_1}{\pi} \tag{12}$$

The local peak value of acceleration within the last three phases occurs at $t = t_5$ and is expressed as:

$$A_{(5-7)}^{\text{peak}} = -\frac{2J_5^{\text{peak}} T_5}{\pi} \tag{13}$$

The peak velocity is reached at $t = t_3$ when the trajectory completes its positive phases for acceleration, and can be identified as:

$$V^{\text{peak}} = V_{\text{st}} + \frac{2J_1^{\text{peak}} T_1}{\pi}(T_1 + T_2) \tag{14}$$

### 2.2. Trajectory smoothness coefficient

As mentioned earlier, in the trajectory planning based on the 7-phase sine jerk model, four time period $T_1$, $T_2$, $T_4$, $T_6$ need to be determined to obtain the final trajectory equation. To facilitate model analysis and trajectory optimization, a parameter $\alpha$ is introduced to represent the ratio of the sine jerk phase time to the entire variable velocity duration:

$$\alpha = \frac{2T_1}{2T_1 + T_2} = \frac{2T_5}{2T_5 + T_6} \tag{15}$$

From Eqs. (12) and (13), it can be seen that if $A_{(1-3)}^{\text{peak}}$ and $A_{(5-7)}^{\text{peak}}$ remain unchanged, $J_1^{\text{peak}}$ and $J_5^{\text{peak}}$ are inversely proportional to $T_1$ and $T_5$, respectively. According to Eq. (15), $T_1$ and $T_5$ are directly proportional to $\alpha$. Consequently, $J_1^{\text{peak}}$ and $J_5^{\text{peak}}$ are inversely proportional to $\alpha$. Therefore, the value of $\alpha$ directly affects the magnitude of jerk. Since jerk is often correlated with the smoothness of the trajectory, the parameter $\alpha$ is referred to as the trajectory smoothness coefficient, which can, to some extent, represent the degree of trajectory smoothness. Generally, the trajectory smoothness requirements for the same task trajectory are identical in both the acceleration and deceleration phases; hence, it is reasonable to use the parameter $\alpha$ in Eq. (15) to simultaneously characterize the smoothness of both the acceleration and deceleration phases.

Based on the trajectory model, it can be readily demonstrated that $\alpha \in [0, 1]$. Setting $\alpha$ to zero leads to $T_1 = T_5 = 0$, which results in the disappearance of the sine jerk phases and the degeneration of the trajectory into a trapezoidal velocity profile. Consequently, the jerk becomes unconstrained, losing its continuity. Conversely, when $\alpha$ is set to one, $T_2 = T_6 = 0$, and the phase of constant acceleration is eliminated. It is apparent that decreasing $\alpha$ enhances the trajectory acceleration capacity at the expense of smoothness, whereas increasing $\alpha$ reduces acceleration capacity but augments smoothness. Adjusting the smoothness coefficient $\alpha$ allows for the modulation of trajectory smoothness, thus harmonizing the trade-off between trajectory speed and accuracy in accordance with task demands. Typically, when the robot has a higher rigidity or the task focuses more on movement speed, $\alpha$ should be minimized to maximize trajectory velocity. On the contrary, when the robot has a lower rigidity or the task emphasizes trajectory accuracy, $\alpha$ should be increased to enhance smoothness. Furthermore, to ensure trajectories with bounded and continuous jerk, $\alpha$ must be non-zero and is thus confined to the range $(0, 1]$.

### 2.3. Equivalent transformation

If only considering the PTP motion of a single joint, the trajectory planning based on the 7-phase sine jerk model is relatively simple and straightforward. However, when this model is extended to multi-joint MP planning, the complexity of the calculations increases significantly. This is due to the fact that the initial and final velocities of each planning segment are typically non-zero, and the synchronization of multi-joint trajectories must also be taken into account. This section presents an in-depth analysis of the 7-phase sine jerk model and explores methods to simplify the model equivalently while maintaining the original constraints, overall trajectory velocity, and trajectory smoothness. The goal is to enhance computational efficiency, ensure the reliability of the 7-phase sine jerk model in online trajectory generation applications, and provide a foundation for subsequent research on trajectory optimization approaches and velocity look-ahead strategies.

From the 7-phase sine jerk model, it is observed that the direction of acceleration is consistent across the first three phases, null during the fourth phase, and uniform in the subsequent three phases. Capitalizing on this pattern, the trajectory is reclassified into three distinct characteristic segments according to the directional attributes of acceleration. The temporal duration, displacement, and terminal velocity for these phases are respectively denoted by $T_{\text{m},k}$, $D_{\text{m},k}$, $v_{\text{m},k}$, where $k = 1, 2, 3$. The total trajectory time and displacement are represented by $T_{\text{m}}$ and $D_{\text{m}}$, respectively. Furthermore, the displacement and velocity at time $t_i$ within the 7-phase sine jerk model are expressed as $d_i = d(t_i)$ and $v_i = v(t_i)$, where $i = 0, 1, \ldots, 7$. With these definitions established, the subsequent relationships can be formulated:

$$T_{\text{m}} = \sum_{k=1}^{3} T_{\text{m},k} \tag{16}$$

$$D_{\text{m}} = \sum_{k=1}^{3} D_{\text{m},k} \tag{17}$$

$$T_{\text{m},1} = 2T_1 + T_2 \tag{18}$$

$$T_{m,2} = T_4 \tag{19}$$

$$T_{m,3} = 2T_5 + T_6 \tag{20}$$

$$D_{m,1} = d_3 - d_0 \tag{21}$$

$$D_{m,2} = d_4 - d_3 \tag{22}$$

$$D_{m,3} = d_7 - d_4 \tag{23}$$

$$v_{m,1} = v_3 \tag{24}$$

$$v_{m,2} = v_4 \tag{25}$$

$$v_{m,3} = v_7 \tag{26}$$

For the first characteristic segment, substitute $\tau_3 = T_1$ into Eq. (7) to obtain $v_3$ and $d_3$, and then calculate the final velocity $v_{m,1}$ and displacement $D_{m,1}$ according to Eqs. (24) and (21):

$$v_{m,1} = v_3 = V_{st} + \frac{2J_1^{peak}}{\pi} T_1 \left(T_1 + T_2\right) \tag{27}$$

$$\begin{aligned} D_{m,1} &= d_3 - d_0 \\ &= V_{st}\left(2T_1 + T_2\right) + \frac{J_1^{peak} T_1}{\pi}\left(2T_1^2 + 3T_1T_2 + T_2^2\right) \end{aligned} \tag{28}$$

Combining Eqs. (15) and (18), $v_{m,1}$ and $D_{m,1}$ can be simplified to:

$$v_{m,1} = V_{st} + \alpha\left(1 - \frac{\alpha}{2}\right)\frac{J_1^{peak}}{\pi} T_{m,1}^2 \tag{29}$$

$$D_{m,1} = V_{st}T_{m,1} + \frac{1}{2}\alpha\left(1 - \frac{\alpha}{2}\right)\frac{J_1^{peak}}{\pi} T_{m,1}^3 \tag{30}$$

Here, a new variable $A_{m,1}$ is introduced and defined as follows:

$$A_{m,1} = \alpha\left(1 - \frac{\alpha}{2}\right)\frac{J_1^{peak}}{\pi} T_{m,1} \tag{31}$$

Then, Eqs. (29) and (30) can be transformed into:

$$v_{m,1} = V_{st} + A_{m,1}T_{m,1} \tag{32}$$

$$D_{m,1} = V_{st}T_{m,1} + \frac{1}{2}A_{m,1}T_{m,1}^2 \tag{33}$$

The expressions of $v_{m,1}$ and $D_{m,1}$ reveal that the motion of the first characteristic segment of the 7-phase jerk model shares the same initial and final velocities, displacement, duration, and average acceleration as the uniformly accelerated motion with acceleration $A_{m,1}$.

Proceeding to the second characteristic segment, by substituting $\tau_4 = T_4$ into Eq. (8), the values for $v_4$ and $d_4$ are derived. Subsequently, using Eqs. (25) and (22), the terminal velocity $v_{m,2}$ and displacement $D_{m,2}$ for this phase can be calculated as:

$$v_{m,2} = v_4 = V_{st} + \frac{2J_1^{peak}}{\pi} T_1 \left(T_1 + T_2\right) \tag{34}$$

$$D_{m,2} = d_4 - d_3 = \left[V_{st} + \frac{2J_1^{peak}T_1}{\pi}\left(T_1 + T_2\right)\right] T_4 \tag{35}$$

By substituting Eqs. (27) and (19) into Eqs. (34) and (35), the resulting expressions are obtained:

$$v_{m,2} = v_{m,1} \tag{36}$$

$$D_{m,2} = v_{m,1}T_{m,2} \tag{37}$$

It is evident that the second characteristic segment of the 7-phase jerk model represents a uniform motion trajectory, with its velocity being equal to the terminal velocity of the first characteristic segment.

Finally, the third characteristic segment is analyzed by substituting $\tau_7 = T_5$ into Eq. (11), which yields the terminal velocity $v_7$ and the total displacement $d_7$ of the 7-phase trajectory. And then, according to Eqs. (26) and (23), the terminal velocity $v_{m,3}$ and displacement $D_{m,3}$ of the third characteristic segment can be calculated as:

$$v_{m,3} = v_7 = V_{st} + \frac{2J_1^{peak}T_1}{\pi}\left(T_1 + T_2\right) - \frac{2J_5^{peak}T_5}{\pi}\left(T_5 + T_6\right) \tag{38}$$

$$\begin{aligned} D_{m,3} = d_7 - d_4 = &\left[V_{st} + \frac{2J_1^{peak}T_1}{\pi}\left(T_1 + T_2\right)\right]\left(2T_5 + T_6\right) \\ &- \frac{J_5^{peak}T_5}{\pi}\left(T_5 + T_6\right)\left(2T_5 + T_6\right) \end{aligned} \tag{39}$$

Incorporating Eqs. (27), (36), (20), and (15), the final velocity $v_{m,3}$ and displacement $D_{m,3}$ can be expressed as follows:

$$v_{m,3} = v_{m,2} - \alpha\left(1 - \frac{\alpha}{2}\right)\frac{J_5^{peak}}{\pi} T_{m,3}^2 \tag{40}$$

$$D_{m,3} = v_{m,2}T_{m,3} - \frac{1}{2}\alpha\left(1 - \frac{\alpha}{2}\right)\frac{J_5^{peak}}{\pi} T_{m,3}^3 \tag{41}$$

Introduce another variable $A_{m,3}$ and define it as follows:

$$A_{m,3} = -\alpha\left(1 - \frac{1}{2}\alpha\right)\frac{J_5^{peak}}{\pi} T_{m,3} \tag{42}$$

Then, Eqs. (40) and (41) can be transformed into:

$$v_{m,3} = v_{m,2} + A_{m,3}T_{m,3} \tag{43}$$

$$D_{m,3} = v_{m,2}T_{m,3} + \frac{1}{2}A_{m,3}T_{m,3}^2 \tag{44}$$

Similarly, from the expressions of $v_{m,3}$ and $D_{m,3}$, it can be seen that the third characteristic segment of the model has the same initial velocity, final velocity, duration, displacement, and average acceleration as the uniformly accelerated motion with acceleration $A_{m,3}$.

By incorporating the terminal velocities defined in Eqs. (32), (36), and (43), and the displacements specified in Eqs. (33), (37), and (44), respectively, a unified expression for the three distinct characteristic segments is established:

$$\begin{cases} v_{m,k} &= v_{m,k-1} + A_{m,k}T_{m,k} \\ D_{m,k} &= v_{m,k-1}T_{m,k} + \frac{1}{2}A_{m,k}T_{m,k}^2 \end{cases} \tag{45}$$

where $k = 1, 2, 3$, and $v_{m,0} = V_{st}$, $A_{m,2} = 0$. Through Eq. (45), it can be clearly seen that the proposed 7-phase sine jerk model is equivalent to the 3-phase trapezoidal velocity model, which is commonly used in trajectory planning, in terms of boundary velocity, time, displacement, and average acceleration. Both models share identical boundary conditions and exhibit similar profiles. Fig. 2 illustrates the equivalence in displacement and velocity between the 7-phase sine jerk model and the trapezoidal velocity model. Leveraging this feature, the complexity of the 7-phase sine jerk model can be reduced by simplifying the model into a 3-phase trapezoidal velocity model, thereby enhancing the computational efficiency of the planning process.

## 3. Trajectory optimization

Given the equivalence between the 7-phase sine jerk model and the 3-phase trapezoidal velocity model, the trajectory generation process in this study is optimized into two steps. Initially, rapid planning is conducted using the equivalent 3-phase trapezoidal velocity model to determine the trajectory time and critical velocities for each characteristic segment. Following this, trajectory interpolation is carried out based on the 7-phase sine jerk model to generate a smooth motion trajectory with continuous jerk. This optimization fully exploits the complementary strengths of both models, ensuring trajectory continuity and substantially improving the computational efficiency of the planning process.

To facilitate the discussion of the proposed trajectory generation method, key parameters involved are first explicitly defined. The trajectory parameters of the proposed 7-phase sine jerk model include:

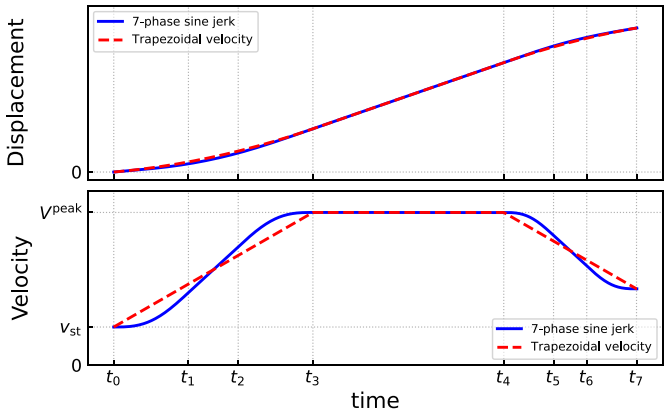


**Fig. 2.** Equivalence between the 7-phase sine Jerk Model and the 3-phase trapezoidal velocity Model.

initial velocity $V_{st}$, maximum final velocity $V_{tg}$, maximum acceleration $A_{max}$, maximum velocity $V_{max}$, total trajectory time $T_m$, total trajectory displacement $D_m$, and trajectory smoothness coefficient $\alpha$. The duration of each phase is denoted as $T_i$, where $i = 1, 2, \ldots, 7$. In addition to the parameters listed above, the equivalent trapezoidal trajectory model also incorporates its own unique parameters, including the time $T_{m,k}$, accelerations $A_{max}$, and displacements $D_{m,k}$, with $k = 1, 2, 3$. The uniform motion during the middle phase of the trapezoidal trajectory results in $A_{m,2} = 0$. To accommodate diverse planning goals, such as time optimization and time synchronization, the acceleration parameters $A_{m,1}$ for the first phase and $A_{m,3}$ for the third phase can take on positive or negative values. In these scenarios, the velocity during the middle phase may not necessarily be the peak velocity of the entire trajectory. Therefore, $V_m$ is introduced to denote the velocity of the uniform motion phase. Additionally, the terminal velocity of the trajectory is represented by $V_{en}$. It is known from Eq. (45) that determining $T_{m,k}$ and $A_{m,k}$ is sufficient to generate the trajectory based on the trapezoidal velocity model. For clarity in explaining the algorithm principle, it is assumed in this paper that all trajectory constraints are valid, meaning that a 3-phase trapezoidal velocity profile satisfying all constraints exists. Special scenarios, such as when the maximum final velocity constraint is unattainable ($V_{tg} > V_{max}$) or the initial velocity exceeds the maximum velocity ($V_{st} > V_{max}$), are beyond the scope of this paper's discussion. Given that robot tasks typically involve unidirectional movement between two waypoints, this paper assumes non-negative values for both displacement and velocity to simplify subsequent problem analysis and description.

The basic mathematical form of the trapezoidal trajectory model in Eq. (45), along with the previously defined relevant parameters, allows for the straightforward derivation of the following mathematical relationships (Biagiotti & Melchiorri, 2008; Siciliano et al., 2009):

$$\begin{cases} V_m = V_{st} + A_{m,1} T_{m,1} \\ V_{en} = V_m + A_{m,3} T_{m,3} \end{cases} \tag{46}$$

$$\begin{cases} D_{m,1} = V_{st} T_{m,1} + \frac{1}{2} A_{m,1} T_{m,1}^2 \\ D_{m,2} = V_m T_{m,2} \\ D_{m,3} = V_m T_{m,3} + \frac{1}{2} A_{m,3} T_{m,3}^2 \end{cases} \tag{47}$$

$$\begin{cases} V_m^2 - V_{st}^2 = 2 A_{m,1} D_{m,1} \\ V_{en}^2 - V_m^2 = 2 A_{m,3} D_{m,3} \end{cases} \tag{48}$$

The 7-phase sine jerk model and the trapezoidal velocity model are interconvertible, yet they exhibit differences in acceleration constraints. Therefore, it is necessary to establish the relationship between the maximum acceleration constraints treated of these two models. As can be inferred from Eqs. (15), (18), and (20):

$$T_1 = \frac{1}{2} \alpha T_{m,1} \tag{49}$$

$$T_5 = \frac{1}{2} \alpha T_{m,3} \tag{50}$$

Further, by combining Eqs. (31), (42), (12), and (13), the relationship between the accelerations of the trapezoidal model and the peak acceleration in the 7-phase sine jerk model can be derived:

$$A_{m,1} = \left(1 - \frac{\alpha}{2}\right) A_{(1-3)}^{peak} \tag{51}$$

$$A_{m,3} = \left(1 - \frac{\alpha}{2}\right) A_{(5-7)}^{peak} \tag{52}$$

Under the condition that the trajectory satisfies the maximum acceleration constraint $A_{max}$, the following inequality is established:

$$A_{(1-3)}^{peak} \le A_{max}, \quad A_{(5-7)}^{peak} \le A_{max} \tag{53}$$

Therefore, the acceleration of the equivalent trapezoidal model should satisfy the following constraint:

$$A_{m,1} \le \left(1 - \frac{\alpha}{2}\right) A_{max}, \quad A_{m,3} \le \left(1 - \frac{\alpha}{2}\right) A_{max} \tag{54}$$

From Eq. (54), it can be observed that the first and third phases of the equivalent trapezoidal model share the same maximum acceleration constraint, here denoted as $A_{MAX}$. Then, the relationship between $A_{MAX}$ and the original maximum acceleration constraint $A_{max}$ can be established as follows:

$$A_{MAX} = \left(1 - \frac{\alpha}{2}\right) A_{max} \tag{55}$$

Consequently, as long as the acceleration of the equivalent trapezoidal trajectory does not exceed $A_{MAX}$, the acceleration of the corresponding trajectory based on the 7-phase sine jerk model will also not exceed $A_{max}$.

### 3.1. Time-optimal trajectory

The time-optimal trajectory planning, based on the 7-phase sine jerk model proposed in this paper, is designed to generate the trajectory with the shortest duration $T_m$ while adhering to constraints on initial velocity $V_{st}$, maximum final velocity $V_{tg}$, maximum acceleration $A_{max}$, maximum velocity $V_{max}$, displacement $D_m$, and trajectory smoothness coefficient $\alpha$. To reduce the complexity of this planning process and improve computational efficiency, the planning is transformed into the time-optimal trajectory planning based on the equivalent trapezoidal model, which also meets the constraints of initial velocity $V_{st}$, maximum terminal velocity $V_{tg}$, maximum acceleration $A_{MAX}$, maximum velocity $V_{max}$, and displacement $D_m$. The latter can be formulated as the following mathematical optimization problem:

Minimize the objective function:

$$T_m = T_{m,1} + T_{m,2} + T_{m,3} \tag{56}$$

subject to:

$$\begin{cases} V_{en} \le V_{tg}, V_m \le V_{max} \\ A_{m,2} = 0, -A_{MAX} \le A_{m,k} \le A_{MAX}, k = 1, 3 \\ D_m = D_{m,1} + D_{m,2} + D_{m,3} \end{cases} \tag{57}$$

To achieve the minimization of the execution time $T_m$, the velocity $V_m$ in the second phase and the velocity $V_{en}$ at the trajectory's end should be as high as possible. However, due to the presence of constraints, the maximum value of $V_m$ must not exceed $V_{max}$, and the maximum value of $V_{en}$ must not exceed $V_{tg}$. According to the relationships Eqs. (46), (47), and (48) of the trapezoidal model and the constraint Eq. (57), the following conditions for determination can be established:

When $D_m \ge \dfrac{V_{tg}^2 - V_{st}^2}{2A_{MAX}}$, the terminal velocity $V_{en}$ can reach the maximum target velocity $V_{tg}$. (58)

When $D_m \ge \dfrac{V_{max}^2}{A_{MAX}} - \dfrac{V_{st}^2 + V_{tg}^2}{2A_{MAX}}$, the intermediate velocity $V_m$ can reach the maximum trajectory velocity $V_{max}$. (59)

**Table 1**
Classification of time-optimal trajectories based on equivalent trapezoidal velocity model.

| No. | Classification criteria | Trajectory expressions |
|---|---|---|
| 1 | $D_{\mathrm{m}} \leq \frac{V_{\mathrm{tg}}^2 - V_{\mathrm{st}}^2}{2A_{\mathrm{MAX}}}$ | $A_{\mathrm{m},1} = A_{\mathrm{MAX}},\ A_{\mathrm{m},3} = 0,\ V_{\mathrm{m}} = V_{\mathrm{en}} = \sqrt{V_{\mathrm{st}}^2 + 2A_{\mathrm{MAX}} D_{\mathrm{m}}}$ |
| 2 | $\frac{V_{\mathrm{tg}}^2 - V_{\mathrm{st}}^2}{2A_{\mathrm{MAX}}} \leq D_{\mathrm{m}} \leq \frac{V_{\mathrm{max}}^2}{A_{\mathrm{MAX}}} - \frac{V_{\mathrm{st}}^2 + V_{\mathrm{tg}}^2}{2A_{\mathrm{MAX}}}$ | $A_{\mathrm{m},1} = A_{\mathrm{MAX}},\ A_{\mathrm{m},3} = -A_{\mathrm{MAX}},\ V_{\mathrm{m}} = \sqrt{A_{\mathrm{MAX}} D_{\mathrm{m}} + \frac{V_{\mathrm{st}}^2 + V_{\mathrm{tg}}^2}{2}},\ V_{\mathrm{en}} = V_{\mathrm{tg}}$ |
| 3 | $D_{\mathrm{m}} \geq \frac{V_{\mathrm{max}}^2}{A_{\mathrm{MAX}}} - \frac{V_{\mathrm{st}}^2 + V_{\mathrm{tg}}^2}{2A_{\mathrm{MAX}}}$ | $A_{\mathrm{m},1} = A_{\mathrm{MAX}},\ A_{\mathrm{m},3} = -A_{\mathrm{MAX}},\ V_{\mathrm{m}} = V_{\mathrm{max}},\ V_{\mathrm{en}} = V_{\mathrm{tg}}$ |

In this study, the trajectory shapes are classified based on these two decision conditions, and the relationships of the trapezoidal trajectory model in Eqs. (46), (47), and (48), along with the constraints of the time-optimal trajectory from Eq. (57), are used to construct a set of equations for each category with variables $V_{\mathrm{m}}$, $V_{\mathrm{en}}$, $A_{\mathrm{m},1}$, $A_{\mathrm{m},3}$, $T_{\mathrm{m},1}$, and $T_{\mathrm{m},3}$. By solving these equations, expressions for the time-optimal trajectories corresponding to each category can be derived. Table 1 provides detailed criteria for different trajectory categories, as well as the calculation expressions for $A_{\mathrm{m},1}$, $A_{\mathrm{m},3}$, $V_{\mathrm{m}}$, and $V_{\mathrm{en}}$.

For each category, $T_{\mathrm{m},1}$ and $T_{\mathrm{m},3}$ can be further calculated using Eq. (46) as follows:

$$T_{\mathrm{m},1} = \frac{V_{\mathrm{m}} - V_{\mathrm{st}}}{A_{\mathrm{m},1}}, \quad T_{\mathrm{m},3} = \frac{V_{\mathrm{en}} - V_{\mathrm{m}}}{A_{\mathrm{m},3}} \tag{60}$$

Based on Eq. (48), the calculation expressions for $D_{\mathrm{m},1}$ and $D_{\mathrm{m},3}$ can be derived as follows:

$$D_{\mathrm{m},1} = \frac{V_{\mathrm{m}}^2 - V_{\mathrm{st}}^2}{2A_{\mathrm{m},1}}, \quad D_{\mathrm{m},3} = \frac{V_{\mathrm{en}}^2 - V_{\mathrm{m}}^2}{2A_{\mathrm{m},3}} \tag{61}$$

By combining Eqs. (47) and (57), the time of the second phase can be calculated as:

$$\begin{aligned} T_{\mathrm{m},2} &= \frac{D_{\mathrm{m},2}}{V_{\mathrm{m}}} = \frac{D_{\mathrm{m}} - D_{\mathrm{m},1} - D_{\mathrm{m},3}}{V_{\mathrm{m}}} \\ &= \frac{D_{\mathrm{m}}}{V_{\mathrm{m}}} - \frac{V_{\mathrm{m}}^2 - V_{\mathrm{st}}^2}{2A_{\mathrm{m},1}V_{\mathrm{m}}} - \frac{V_{\mathrm{en}}^2 - V_{\mathrm{m}}^2}{2A_{\mathrm{m},3}V_{\mathrm{m}}} \end{aligned} \tag{62}$$

After determining the parameters $T_{\mathrm{m},k}$ and $A_{\mathrm{m},k}$ of the trapezoidal trajectory, the necessary parameters for the 7-phase sine jerk model can be calculated by utilizing the relationship between this model and the 3-phase trapezoidal velocity model. The relationships for the durations of each phase in both trajectory models can be obtained from Eqs. (15), (18), (19), and (20):

$$\begin{cases} T_1 = \frac{\alpha T_{\mathrm{m},1}}{2} \\ T_2 = (1-\alpha) T_{\mathrm{m},1} \\ T_4 = T_{\mathrm{m},2} \\ T_5 = \frac{\alpha T_{\mathrm{m},3}}{2} \\ T_6 = (1-\alpha) T_{\mathrm{m},3} \end{cases} \tag{63}$$

The peak jerk calculation expression for the 7-phase sine jerk model can be derived from Eqs. (31) and (42):

$$J_1^{\mathrm{peak}} = \frac{\pi A_{\mathrm{m},1}}{\alpha(1-\alpha) T_{\mathrm{m},1}}, \quad J_5^{\mathrm{peak}} = -\frac{\pi A_{\mathrm{m},3}}{\alpha(1-\alpha) T_{\mathrm{m},3}} \tag{64}$$

At this point, all parameters of the proposed 7-phase sine model have been successfully determined, including the time distribution of each phase and the peak jerk values. By incorporating the trajectory model expressions outlined in Section 2.1, the time-optimal trajectory based on the 7-phase sine jerk model can be derived.

It is worth noting that, as evident from Eq. (64), unlike common trajectory models based on constant jerk constraints, the peak jerks $J_1^{\mathrm{peak}}$ and $J_5^{\mathrm{peak}}$ of the trajectory model proposed in this paper are adaptively computed based on the phase times $T_{\mathrm{m},1}$ and $T_{\mathrm{m},3}$ as well as other fixed parameters. This adaptive adjustment characteristic forms the core basis for the equivalence between the 3-phase trapezoidal velocity model and the 7-phase sine jerk model. It is due to the adaptive adjustment of peak jerks that these two models share the same average acceleration, which is a key commonality between them. Given that the absolute value of acceleration in the trapezoidal velocity model is fixed at $A_{\mathrm{MAX}}$, the equivalent 7-phase sine jerk model also exhibits a constant absolute value of average acceleration $A_{\mathrm{MAX}}$ in time-optimal trajectory planning. This suggests that under varying path conditions, regardless of variations in the density of path control points, the proposed 7-phase sine jerk model can maintain stable acceleration, thereby preserving consistent time efficiency.

### 3.2. Time-synchronized trajectory

In the trajectory planning for multi-joint robots, it is necessary to consider the issue of trajectory synchronization due to the independent control of each joint. The kinematic constraints of individual joints typically vary, resulting in different trajectory durations for each joint. To alleviate the burden on the joint actuators and achieve a smoother motion, actuators with higher velocities often need to decelerate, thereby generating time-synchronized trajectories based on the longest trajectory time among all joints.

Time-synchronized trajectory planning introduces an additional total time constraint denoted as $T_{\mathrm{m}}$ while adopting an equivalent model conversion strategy similar to the time-optimal trajectory generation. In this planning process, the equivalent trapezoidal velocity model must satisfy various constraints, including initial velocity $V_{\mathrm{st}}$, maximum final velocity $V_{\mathrm{tg}}$, maximum acceleration $A_{\mathrm{MAX}}$, maximum velocity $V_{\mathrm{max}}$, total displacement $D_{\mathrm{m}}$, and the reference total trajectory time $T_{\mathrm{m}}$.

The function $s(\Delta t)$ is defined to represent the displacement generated by the equivalent trapezoidal trajectory after a time shift $\Delta t$, where $\Delta t$ is the time elapsed relative to the starting time of the trajectory and $\Delta t \in [0, T_{\mathrm{m}}]$. Therefore, $s(T_{\mathrm{m}})$ denotes the displacement of the synchronized trajectory corresponding to the reference total time $T_{\mathrm{m}}$. During the generation of synchronized trajectories, the potential trajectories are classified into multiple categories based on different expressions of $s(t)$, while satisfying all constraints except for the total displacement $D_{\mathrm{m}}$. The collection of ranges of $s(T_{\mathrm{m}})$ corresponding to these categories should fully cover all possible values of $s(T_{\mathrm{m}})$, with non-overlapping ranges for each category. Additionally, in dealing with MP trajectory planning problems, to ensure trajectory continuity, it is necessary to ensure that the final velocity of the current trajectory segment is the same as the initial velocity of the next trajectory segment. Therefore, when classifying potential synchronized trajectories, priority is given to the classification method that maximizes the final velocity $V_{\mathrm{en}}$, in order to increase the initial velocity of the subsequent trajectory segment as much as possible while meeting the current trajectory synchronization requirements. This can minimize the velocity reduction caused by time synchronization, thereby ensuring time optimality for each sub-trajectory segment by maximize its initial velocity. Table 2 details the classification of potential trapezoidal synchronized trajectories. The column labeled "Classification Criteria" outlines the specific constraints under which each category is valid, and when combined with the original trajectory constraints, determine the unique trajectory expression for each category. The column titled "Boundary Condition" provides the variable parameter and its ranges within each category. The column named "Trajectory Expression" presents the calculation expressions for key parameters in each category. For the trapezoidal velocity model, the calculations for each category only require solving equations no higher than quadratic. Therefore, to avoid taking up too

**Table 2**
Classification of time-synchronized trajectories based on equivalent trapezoidal velocity model.

| No. | Classification criteria | Boundary conditions | Trajectory expressions |
|---|---|---|---|
| 1 | $\frac{V_{st}+V_{tg}}{A_{MAX}} \le T_m,\ A_{m,1}=-A_{MAX},\ A_{m,3}=A_{MAX}$ | $T_{m,3} \in \left[0,\ \frac{V_{tg}}{A_{MAX}}\right]$ | $V_m=0,\ V_{en}=A_{MAX}T_{m,3}$ |
| 2 | $\frac{V_{st}+V_{tg}}{A_{MAX}} \le T_m,\ A_{m,1}=-A_{MAX},\ V_m=0,\ V_{en}=V_{tg}$ | $T_{m,3} \in \left[\frac{V_{tg}}{A_{MAX}},\ T_m-\frac{V_{st}}{A_{MAX}}\right]$ | $A_{m,3}=\frac{V_{en}}{T_{m,3}}$ |
| 3 | $\frac{V_{st}+V_{tg}}{A_{MAX}} \le T_m,\ A_{m,1}=-A_{MAX},\ V_{en}=V_{tg},\ T_{m,2}=0$ | $V_m \in [0,\ V_{st}]$ | $A_{m,3}=\frac{(V_{en}-V_m)A_{MAX}}{A_{MAX}T_m-V_{st}+V_m}$ |
| 4 | $\frac{V_{st}+V_{tg}}{A_{MAX}} \ge T_m \ge \frac{V_{st}}{A_{MAX}},\ A_{m,1}=-A_{max},\ A_{m,3}=A_{max},\ V_m=0$ | $T_{m,3} \in \left[0,\ T_m-\frac{V_{st}}{A_{MAX}}\right]$ | $V_{en}=A_{MAX}T_{m,3}$ |
| 5 | $\frac{V_{st}+V_{tg}}{A_{MAX}} \ge T_m \ge \frac{V_{tg}-V_{st}}{A_{MAX}},\ \frac{V_{st}}{A_{MAX}} \le T_m,\ A_{m,1}=-A_{MAX},\ A_{m,3}=A_{MAX},\ T_{m,2}=0$ | $V_m \in \left[0,\ \frac{V_{st}+V_{tg}-A_{MAX}T_m}{2}\right]$ | $V_{en}=A_{MAX}T_m+2V_m-V_{st}$ |
| 6 | $\frac{V_{st}+V_{tg}}{A_{MAX}} \ge T_m \ge \frac{V_{tg}-V_{st}}{A_{MAX}},\ \frac{V_{st}}{A_{MAX}} \le T_m,\ A_{m,1}=-A_{MAX},\ V_{en}=V_{tg},\ T_{m,2}=0$ | $V_m \in \left[\frac{V_{st}+V_{tg}-A_{MAX}T_m}{2},\ V_{st}\right]$ | $A_{m,3}=\frac{(V_{en}-V_m)A_{MAX}}{A_{MAX}T_m-V_{st}+V_m}$ |
| 7 | $\frac{V_{tg}-V_{st}}{A_{MAX}} \ge T_m \ge \frac{V_{st}}{A_{MAX}},\ A_{m,1}=-A_{MAX},\ A_{m,3}=A_{MAX},\ T_{m,2}=0$ | $V_m \in [0,\ V_{st}]$ | $V_{en}=A_{MAX}T_m+2V_m-V_{st}$ |
| 8 | $\frac{V_{st}}{A_{MAX}} \ge T_m \ge \frac{V_{tg}-V_{st}}{A_{MAX}},\ A_{m,1}=-A_{MAX},\ A_{m,3}=A_{MAX}$ | $V_{en} \in [V_{st}-A_{MAX}T_m,\ V_{tg}]$ | $V_m=\frac{V_{st}+V_{en}-A_{MAX}T_m}{2}$ |
| 9 | $\frac{V_{st}}{A_{MAX}} \ge T_m \ge \frac{V_{tg}-V_{st}}{A_{MAX}},\ A_{m,1}=-A_{MAX},\ V_{en}=V_{tg}$ | $V_m \in \left[\frac{V_{st}+V_{tg}-A_{MAX}T_m}{2},\ V_{st}\right]$ | $A_{m,3}=\frac{(V_{tg}-V_m)A_{MAX}}{A_{MAX}T_m-V_{st}+V_m}$ |
| 10 | $\frac{2V_{max}-V_{st}-V_{tg}}{A_{MAX}} \le T_m,\ A_{m,1}=A_{MAX},\ V_{en}=V_{tg},\ T_2=0$ | $V_m \in [V_{st},\ V_{max}]$ | $A_{m,3}=\frac{(V_{tg}-V_m)A_{MAX}}{A_{MAX}T_m-V_m+V_{st}}$ |
| 11 | $\frac{2V_{max}-V_{st}-V_{tg}}{A_{MAX}} \le T_m,\ A_{m,1}=A_{MAX},\ V_m=V_{max},\ V_{en}=V_{tg}$ | $T_{m,2} \in \left[0,\ T_m-\frac{2V_{max}-V_{st}-V_{tg}}{A_{MAX}}\right]$ | $A_{m,3}=\frac{V_{max}-V_{tg}}{T_{m,3}}$ |
| 12 | $\frac{2V_{max}-V_{st}-V_{tg}}{A_{MAX}} \ge T_m \ge \frac{V_{tg}-V_{st}}{A_{MAX}},\ A_{m,1}=A_{MAX},\ V_{en}=V_{tg}$ | $V_m \in \left[V_{st},\ \frac{V_{st}+V_{tg}+A_{MAX}T_m}{2}\right]$ | $A_{m,3}=\frac{(V_{tg}-V_m)A_{MAX}}{A_{MAX}T_m-V_m+V_{st}}$ |

much space, this paper omits the detailed derivation process of the trajectory expressions for each category.

In trapezoidal synchronized trajectory calculation, the first step is to assess the validity of each category in Table 2 based on the classification criteria. Subsequently, for the valid categories, the range of values for $s\left(T_m\right)$ is calculated by considering the boundary conditions, and the category that can cover the target total displacement $D_m$ is identified. Then, the specific value of the variable parameter for this category is determined by solving the equation $s\left(T_m\right)=D_m$, thereby obtaining the final trajectory. It is important to note that if a category matching $D_m$ cannot be found in Table 2, it indicates the inability to generate the trajectory with duration $T_m$, resulting in trajectory synchronization failure. This is a common occurrence in multi-joint MP trajectory planning. In case of trajectory synchronization failure, the trajectory constraints must be adjusted through corresponding strategies in global velocity optimization, followed by another attempt to generate the synchronized trajectory. The methods for handling synchronization failures will be discussed later in this paper.

After successfully identifying the trajectory category, the same method used for the time-optimal trajectory derivation is employed to construct the time-synchronized trajectory based on the 7-phase sine jerk model. Firstly, by analyzing the calculation expressions in Table 2, the key parameters of the trapezoidal model can be precisely determined, including the mid-phase velocity $V_m$, the final velocity $V_{en}$, and the accelerations $A_{m,1}$, $A_{m,2}$, $A_{m,3}$ for each phase. The phase times $T_{m,k}$ of the trapezoidal model trajectory are calculated using Eqs. (60) and (62). Subsequently, by substituting these time parameters into Eqs. (63) and (64), all the trajectory parameters required to construct the 7-phase sine jerk model can be obtained. Combining this with the trajectory model formulas introduced in Section 2.1 yields the time-synchronized trajectory based on the 7-phase sine jerk model.

## 4. Multi-joint multi-point trajectory velocity look-ahead

In MP trajectory planning, velocity look-ahead technology plays a crucial role (Hu et al., 2006; Tsai et al., 2010; Ye et al., 2008). By analyzing future motion states in advance, it optimizes the current trajectory to adapt to upcoming motion requirements. This approach significantly improves the continuity, smoothness, and execution efficiency of the MP trajectory. Velocity look-ahead technology can be categorized into global velocity look-ahead (Wang & Yau, 2009) and local velocity look-ahead (Li et al., 2019). Global velocity look-ahead completes trajectory planning for all paths at once by analyzing the motion states of the entire future trajectory. However, when there is a large number of path control points, long time for planning calculations may affect the response speed of motion commands. In contrast, local velocity look-ahead analyzes only a portion of the future trajectory segments based on the predefined velocity look-ahead depth, ensuring trajectory continuity and improving real-time trajectory planning. This paper combines local velocity look-ahead technology with trajectory generation methods to propose a MP trajectory velocity look-ahead strategy for multi-joint robotic manipulators, optimizing time efficiency and achieving time-optimal MP trajectory planning.

Positive integers $n$ and $w$ are used to represent the number of joints and the number of path control points in a multi-joint robotic manipulator, where $n>1$ and $w>1$. The position of the $j$th point of the $i$th joint is denoted by $P_{i,j}$, where $i=1,2,\ldots,n$ and $j=0,1,\ldots,w-1$. Specifically, $P_{i,0}$ and $P_{i,w-1}$ indicate the starting and ending positions of the $i$th joint in the MP trajectory. $V_{max,i}$, $A_{max,i}$, and $\alpha_i$ represent the maximum velocity constraint, the maximum acceleration constraint, and the trajectory smoothing coefficient for joint $i$, respectively. The symbol $d$ is used to denote the preset velocity look-ahead depth.

Fig. 3 details the velocity look-ahead strategy process in the multi-joint MP trajectory planning proposed in this study. After determining the manipulator's path control points and kinematic constraints, a positive integer variable $k$ is used to identify the target point index for each sub-trajectory segment. The planning of $w-1$ sub-trajectory segments is completed through an iteration of $k$ from 1 to $w-1$. In the planning of each sub-trajectory segment, the variable $g$ represents the index of the target point predicted in the look-ahead calculation, and the value of g must not exceed the minimum value between $k+d$ and $w-1$ to ensure that the predicted target point does not exceed the maximum range of the trajectory.

The planning of each sub-trajectory segment includes two stages in chronological order: backward planning and forward planning. In the backward planning stage, starting from the furthest target point allowed by the look-ahead depth to the end point of the current sub-trajectory segment, the time-optimal trajectory planning is conducted along the path in the backward direction for each joint of the manipulator with an initial velocity of zero; simultaneously, the maximum velocities of the path control points that are passed through are calculated, which will be used to limit the velocity of that point in the forward planning. The maximum final velocity constraint of the $i$th joint's $g$th segment trajectory obtained during the backward planning process is represented by ${}^{b}v_{i,g}$. In the forward planning stage, the initial velocity of the first sub-trajectory segment is set to zero,

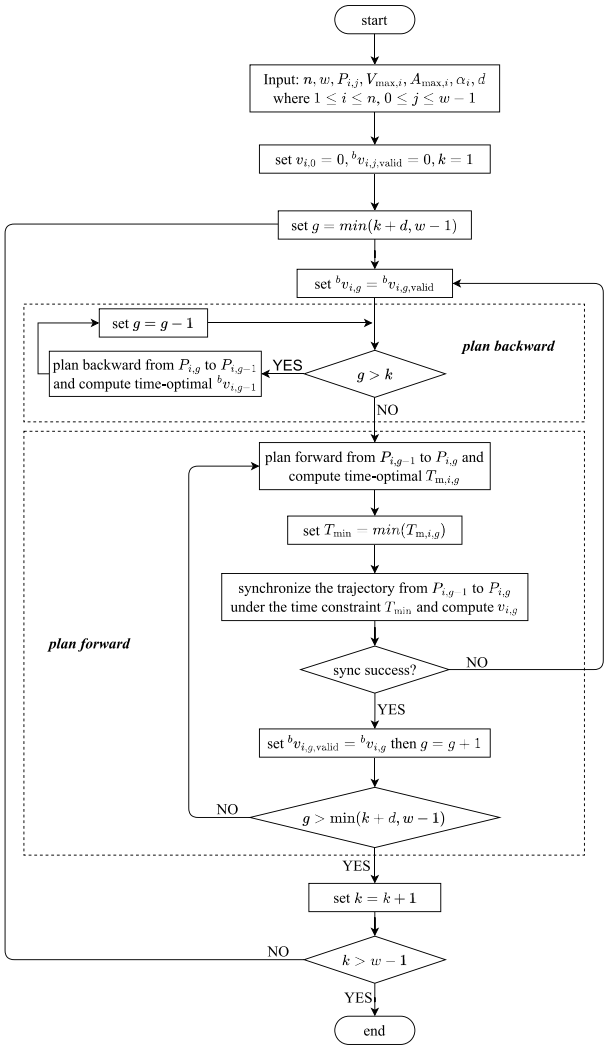


**Fig. 3.** Flowchart of the multi-joint multi-point trajectory velocity look-ahead process.

with subsequent segments using the final velocity of the previous segment as the initial velocity. Starting from the beginning of the current sub-trajectory segment and extending to the farthest target point allowed by the look-ahead depth, the time-optimal trajectory planning is conducted along the path in the forward direction, with trajectory synchronization for each joint performed at each path control point. The actual final velocity of the $i$th joint in the $g$th sub-trajectory segment is defined as $v_{i,g}$, which is obtained after the completion of trajectory synchronization during the forward planning process.

It is worth noting that whether in forward planning or backward planning, the entire calculation process must adhere to the kinematic constraints specified by the task or the robotic manipulator, including maximum velocity $V_{\max,i}$, maximum acceleration $A_{\max,i}$, and smoothing coefficient $\alpha_i$, etc. Additionally, if adjacent trajectory segments have opposite motion directions, the instantaneous velocity, acceleration, and jerk at the critical points of these two segments are set to zero to ensure continuity when the motion direction changes and to avoid unnecessary overshoot or undershoot at the critical points, thereby ensuring trajectory accuracy and reducing the risk of robot collisions.

To address potential trajectory synchronization failures in the velocity look-ahead process, for all path control points, the variable ${}^{b}v_{i,j,\text{valid}}$ is introduced to store the value of ${}^{b}v_{i,j}$ used during the most recent successful synchronization for the $j$th sub-trajectory segment, with its initial value set to zero. If synchronization failure occurs in the $j$th sub-trajectory segment during a velocity look-ahead process, the value of ${}^{b}v_{i,j,\text{valid}}$ is directly substituted for ${}^{b}v_{i,j}$. Subsequently, the endpoint of the $j$th sub-trajectory segment is set as the furthest look-ahead target point, and the current velocity look-ahead planning is re-executed to resolve the synchronization issue in that trajectory segment. The setting of the variable ${}^{b}v_{i,j,\text{valid}}$ provides a feasible alternative for multi-joint trajectory synchronization, ensuring that the algorithm can quickly revert to the most recent valid planning state in the event of synchronization failure, thereby guaranteeing the robustness of the algorithm.

By adjusting the look-ahead depth $d$, the trade-off between computational efficiency and trajectory speed can be balanced. Specifically, increasing the look-ahead depth $d$ will prolong the computation time, which may have a negative impact on the real-time nature of the planning. However, the benefit is the ability to obtain a higher-speed MP trajectory, thereby reducing the total execution time of the trajectory. Conversely, reducing the look-ahead depth $d$ can improve computational efficiency and enhance system real-time performance to a certain extent, but may sacrifice the overall speed of the trajectory, leading to an increase in the total trajectory time. Therefore, the value of the look-ahead depth $d$ should be determined by comprehensively consider the requirements of execution efficiency and the computational capabilities of the controller to achieve the optimal balance between trajectory speed and real-time performance of planning. When all sub-trajectory segments have been traversed, i.e., $k > w-1$, it indicates that the planning of the entire MP trajectory of the multi-joint robot has been successfully completed.

The velocity look-ahead method for multi-joint MP trajectories proposed in this study mainly consists of two key steps: backward planning and forward planning. The core objective of backward planning is to determine the maximum end velocity of each joint in the current sub-trajectory segment being planned based on the look-ahead path depth. The goal of forward planning is to generate synchronized trajectories for each joint with minimum time and maximum final velocity in the current sub-trajectory segment, based on the maximum final velocity constraints obtained from the backward planning. Trajectory synchronization is only performed in the forward planning stage and full consideration is given to remedial measures in case of synchronization failure. Through this method, it is possible to effectively generate time-optimal MP synchronized trajectories for multi-joint robotic manipulators in real-time while satisfying the kinematic constraints.

## 5. Results and discussion

In this section, the proposed multi-joint MP trajectory planning method is validated through simulation and physical experiments. The algorithm is implemented in the C programming language to ensure the efficiency and reliability of the code, and the trajectory data generated by the algorithm is visualized using the Python language.

### 5.1. Simulations

To validate the effectiveness of the proposed algorithm from multiple perspectives, simulations were conducted on a personal computer equipped with a 1.60 GHz Intel Core i5-8250U CPU and 16 GB RAM.

#### 5.1.1. Single joint

Task 1 is based on time-optimal PTP motion of a single joint to validate the effectiveness of the proposed trajectory planning method. The initial position of the joint is set at 15°, and it is required to move to the target position of 100° as quickly as possible at different trajectory smoothing coefficients $\alpha$. During this process, the maximum velocity and acceleration constraints are set at 100 deg/s and 150 deg/s$^2$, respectively. Fig. 4 illustrates the position, velocity, acceleration, and jerk profiles of the joint for trajectory smoothing coefficients $\alpha$ of 0.25, 0.5, 0.75, and 1.0, respectively. By comparing the profiles in the figure,

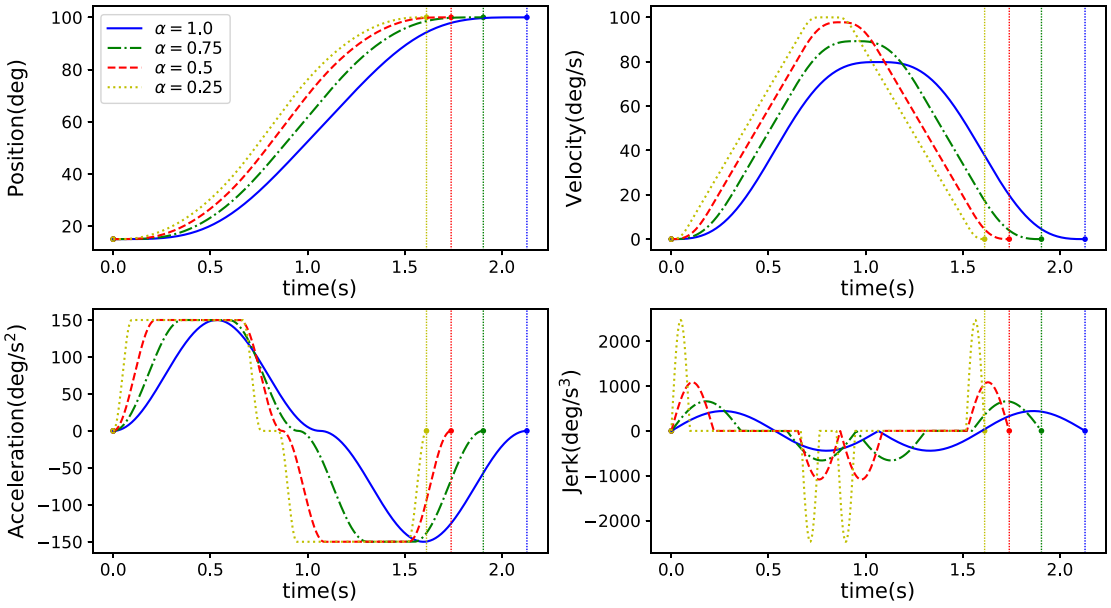


**Fig. 4.** Joint position, velocity, acceleration and jerk profiles in task 1.

the significant impact of the value of $\alpha$ on the velocity, total motion time, and smoothness of the trajectory can be observed. A smaller $\alpha$ results in higher velocity and shorter motion time. In particular, the trajectory corresponding to $\alpha = 0.25$ has the shortest motion time and includes a phase of constant velocity, which matches the maximum velocity constraint. The peak acceleration of all trajectories meets the predefined maximum acceleration constraint, while the peak jerk tends to increase as $\alpha$ decreases due to the adaptive computation mechanism. This trend indicates that the $\alpha$ value is negatively correlated with trajectory velocity and positively correlated with trajectory smoothness. Furthermore, the jerk profiles of the four trajectories are bounded and continuous, demonstrating the effectiveness of the adaptive calculation of peak jerk acceleration in the proposed algorithm. In summary, the simulation in task 1 has confirmed the effectiveness of the proposed trajectory planning method under different trajectory smoothing coefficients and revealed the influence of the trajectory smoothing coefficient values on trajectory characteristics.

The objective of task 2 is to validate the effectiveness of the proposed trajectory planning method in generating time-optimal MP trajectories for a single joint, and to evaluate its acceleration performance under different path conditions. In this task, the kinematic constraints are kept consistent with task 1, and the starting and ending points of the path remain unchanged. As shown in Table 3, four paths of equal length but with different path characteristics are constructed by inserting varying numbers of waypoints between the start and end points. This design facilitates a direct comparison of the acceleration performance of the proposed trajectory planning method in handling paths of different complexities. To ensure the consistency of testing conditions, the trajectory smoothing coefficient $\alpha$ for all paths is set to 0.75. Additionally, the look-ahead depth $d$ is uniformly set to 10. This configuration ensures that all test paths have the same look-ahead distance, regardless of the number of trajectory segments, effectively avoiding potential interference of look-ahead depth on the test results of acceleration performance.

Fig. 5 shows the positions, velocities, accelerations, and jerk profiles for these four paths. All trajectories comply with the specified kinematic constraints, and the jerk profiles remain continuous throughout the entire trajectory period. Notably, as the number of path control points increases, the frequency and amplitude of trajectory fluctuations also increase; however, the execution time of all trajectories remains consistent at 1.9048 s. This result fully confirms that the proposed trajectory planning method can maintain a constant acceleration capability under different path complexity conditions. Especially when it is necessary to increase path control points to improve process accuracy, the execution efficiency can still be maintained, significantly enhancing the robot's application value in high-accuracy manufacturing processes and providing greater flexibility for the optimization of production processes.

**Table 3**
Joint positions of the path control points for the single-joint multi-point motion in task 2.

| Path No. | Positions (deg) | Number of points |
|---|---|---|
| 1 | 15, 100 | 2 |
| 2 | 15, 41, 72, 100 | 4 |
| 3 | 15, 30, 45, 69, 85, 100 | 6 |
| 4 | 15, 20, 34, 48, 66, 80, 88, 95, 100 | 9 |

It should be noted here that multi-joint motion is not used for testing when verifying the constant acceleration capability of the proposed method. This is because trajectory synchronization issues in multi-joint motion may interfere with the acceleration performance, making it difficult to compare the acceleration performance of the trajectory planning algorithm on paths with different complexity. In contrast, motion based on single-joint can effectively avoid the problem of trajectory synchronization, allowing the total execution time on different paths to directly reflect the acceleration performance of the algorithm.

### 5.1.2. *Multiple joints*

For time-optimal multi-joint PTP motion, this work selects a 6-DOF serial manipulator as the validation object and conducts simulations on the proposed trajectory planning method in task 3. To comprehensively evaluate the performance of the proposed method, it is compared against several jerk-continuous trajectory planning methods proposed in earlier studies, including the seventh-order polynomial (Angeles, 2014), 3-phase sine jerk (Valente et al., 2017), and 15-phase sine jerk trajectories (Fang et al., 2020). Table 4 details the joint position data and corresponding kinematic constraint conditions used for testing. It is worth noting that although the jerk constraint originating from the benchmark works is listed in the table, it does not apply to the approach proposed in this study. This is because the proposed method can automatically calculate the optimal peak jerk in time-optimal and

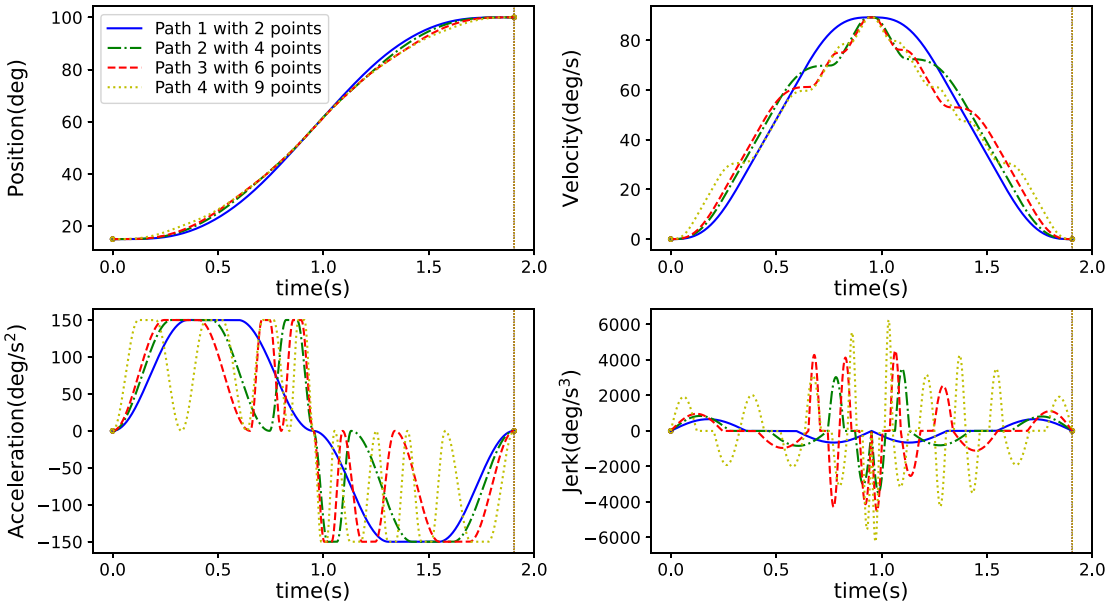


**Fig. 5.** Joint position, velocity, acceleration and jerk profiles ($\alpha = 0.75$) in task 1.

**Table 4**
Joint positions of the path and kinematic limits for the multi-joint point-to-point motion in task 3.

| | | Joint No. | | | | | |
|---|---|---|---|---|---|---|---|
| | | 1 | 2 | 3 | 4 | 5 | 6 |
| Positions | Start Point | −10 | 20 | 15 | 150 | 30 | 120 |
| | End Point | 55 | 35 | 30 | 10 | 70 | 25 |
| Necessary Constraints | Velocity (deg/s) | 100 | 95 | 100 | 150 | 130 | 110 |
| | Acceleration (deg/s$^2$) | 60 | 60 | 75 | 70 | 90 | 80 |
| Optional Constraints | Jerk (deg/s$^3$) | 60 | 66 | 85 | 70 | 75 | 70 |

**Table 5**
Comparison of optimal execution times for the multi-joint point-to-point motions in task 3.

| Work | Motion profile | Execution time (s) |
|---|---|---|
| Angeles (2014) | 4-5-6-7 Polynomial | 4.7177 |
| Valente et al. (2017) | 3-phase sine jerk | 4.6498 |
| Fang et al. (2020) | 15-phase sine jerk | 4.0922 ($\alpha$ = 0.1) |
| | | 4.3875 ($\alpha$ = 0.5) |
| | | 4.6498 ($\alpha$ = 1.0) |
| Present | 7-phase sine jerk | 2.9024 ($\alpha$ = 0.1) |
| | | 3.2664 ($\alpha$ = 0.5) |
| | | 4.0004 ($\alpha$ = 1.0) |

time-synchronized trajectory planning without the need for additional jerk constraint conditions. Therefore, the presence of the jerk constraint in the table is solely for the benchmark methods used for comparison.

As outlined in the preceding sections, the trajectory smoothing coefficient $\alpha$ plays a crucial role in adjusting the speed and smoothness of robotic trajectories. Table 5 summarizes the optimal execution times of the manipulator obtained using different trajectory planning techniques in task 3. It is important to note that the ramp coefficient $\alpha$ used in Fang et al. (2020) has a similar effect on trajectory smoothness and speed as the trajectory smoothing coefficient $\alpha$ introduced in this paper, and they have the same value range. As the value of $\alpha$ increases, higher priority is given to trajectory smoothness, with a corresponding reduction in trajectory speed.

From the test results, the method proposed in Fang et al. (2020), when the ramp coefficient $\alpha$ is set to 0.1, demonstrates the fastest execution speed among all benchmark methods, achieving the trajectory time of 4.0922 s. Using this as a reference, the method proposed in this study, when the trajectory smoothing coefficient is set to 0.1, reduces the trajectory time by 29.1% (from 4.0922 s to 2.9024 s); even when the trajectory smoothing coefficient is set to 1.0, that is, when the trajectory speed has the lowest priority, the trajectory time is still reduced by 2.2% (from 4.0922 s to 4.0004 s). Therefore, the results show that the proposed trajectory planning method effectively enhances trajectory velocity and reduces trajectory time through adaptive peak jerk calculation.

Fig. 6 details the joint position, velocity, acceleration, and jerk profiles planned using the method proposed in this study with $\alpha$ set to 0.5 for the time-optimal multi-joint PTP motion in task 3. These plots clearly demonstrate that all motion profiles maintain good continuity throughout the entire motion process, ensuring the sufficient smoothness of the time-optimal trajectories. The joints exhibit a monotonic and stable trend as they reach the desired positions, without any oscillation.

Addressing the problem of time-optimal multi-joint MP trajectory planning, four path control points for a 6-DOF manipulator, as illustrated in Table 6, are selected for testing in task 4. Kinematic constraints still follow the data from Table 4, with the look-ahead depth d set to 10, exceeding the number of sub-trajectories to maximize the look-ahead performance. In this task, the trajectory smoothing coefficient $\alpha$ is set to 0.1, 0.5, and 1.0, respectively, to evaluate the impact of different parameter settings on trajectory execution efficiency. Considering that the method proposed in Wu et al. (2023) can achieve full jerk continuity for the entire trajectory in multi-joint MP trajectory planning, without overshoot and oscillation during trajectory execution, a comparison is made between this method and the algorithm proposed in this study in terms of trajectory time to verify the performance of the proposed algorithm in motion speed.

Table 7 presents the comparison results of trajectory times obtained using these two methods. The method introduced in this study, with $\alpha$ values of 0.1, 0.5, 0.75, and 1.0, respectively, reduces the trajectory

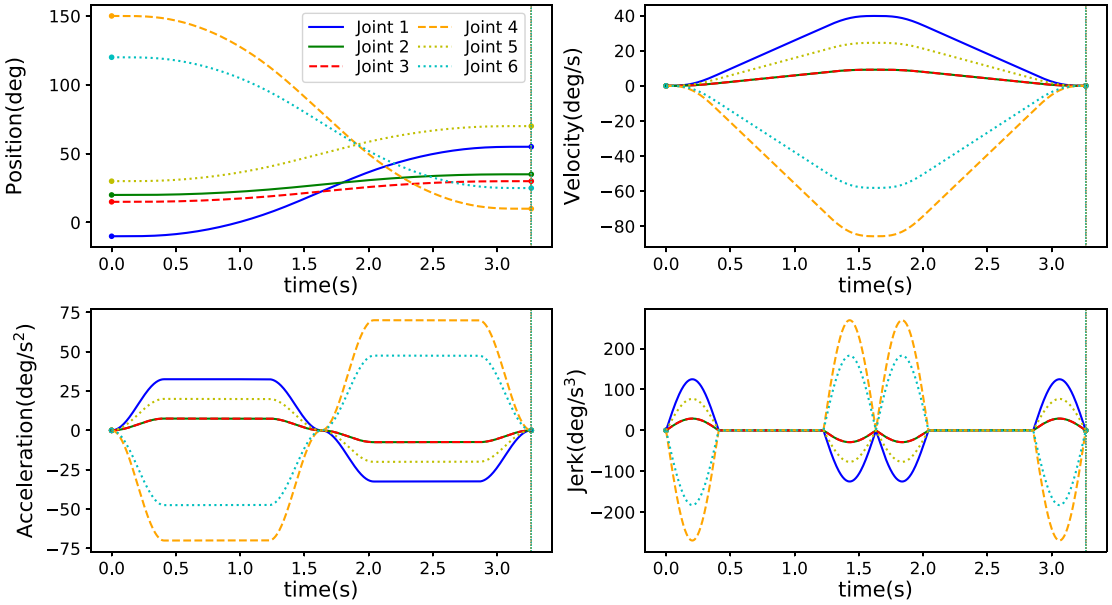


**Fig. 6.** Time-optimal multi-joint point-to-point motion profiles resulted from the proposed method in task 3 ($\alpha = 0.5$).

**Table 6**
Positions of the path control points for the time-optimal multi-joint multi-point motion in task 4.

| Point No. | Joint No. (deg) | | | | | |
|---|---|---|---|---|---|---|
| | 1 | 2 | 3 | 4 | 5 | 6 |
| 1 | −10 | 20 | 15 | 150 | 30 | 120 |
| 2 | 60 | 50 | 100 | 100 | 110 | 60 |
| 3 | 20 | 120 | −10 | 40 | 90 | 100 |
| 4 | 55 | 35 | 30 | 10 | 70 | 25 |

**Table 7**
Comparison of optimal execution times for the multi-joint multi-point motions in task 4.

| Work | Trajectory planning method | Execution time (s) |
|---|---|---|
| Wu et al. (2023) | piecewise motion profile and series–parallel analytical strategy | 12.304 |
| Present | 7-phase sine jerk and velocity look-ahead strategy | 7.144 ($\alpha = 0.1$) |
| | | 8.041 ($\alpha = 0.5$) |
| | | 8.808 ($\alpha = 0.75$) |
| | | 9.848 ($\alpha = 1.0$) |

time by 41.9% (from 12.304 s to 7.144 s), 34.6% (from 12.304 s to 8.041 s), 28.4% (from 12.304 s to 8.808 s), and 20.0% (from 12.304 s to 9.848 s) compared to the method from Wu et al. (2023). These results demonstrate that the proposed algorithm offers a significant advantage in enhancing the motion speed of the multi-joint MP trajectory planning.

Fig. 7 illustrates the trajectory position, velocity, acceleration, and jerk profiles of the multi-joint MP trajectory in task 4 obtained using the proposed planning method with $\alpha$ set to 0.75. The figure indicates the exact moments at which each joint passes through the path control points. By observing these curves, it is evident that the motion trajectories of all joints exhibit excellent continuity and achieve precise time synchronization at the four path control points. This result strongly demonstrates the effectiveness of the proposed algorithm in addressing complex multi-joint MP trajectory planning problems.

### 5.2. Experiments

In order to further validate the practicality of the proposed method, experiments were carried out in task 5 on a 6-DOF SIASUN manipulator T12B-14, as shown in Fig. 8. These experiments utilize the same path control points and adhere to the same kinematic constraints as those in task 4. The system control cycle and trajectory interpolation cycle of this manipulator are both set to 0.004s, and the actual positions of each joint can be measured using the built-in encoders of the motors. Table 8 summarizes the maximum absolute values of the position tracking errors of each joint and the execution time of the task under different trajectory smoothing coefficients. The results reveal a positive correlation between the position tracking error and the trajectory speed with the adjustment of the trajectory smoothing coefficient. When the trajectory smoothing coefficient $\alpha$ is set to 1.0, a comparison of the planning positions, the actual measured positions, and the tracking errors of each joint is presented in Fig. 9. It is evident from the figure that the actual measured curves closely align with the planning ones, with only minor deviations attributed to slight time delays introduced from data transmission and the PID configuration; and the final positioning errors at the target points approach zero. Overall, the experimental results are satisfactory, providing strong evidence for the effectiveness and practicality of the proposed method in this study.

## 6. Conclusion

This study proposes a time-optimal multi-joint MP trajectory planning method, providing an efficient and reliable solution for high-speed and high-accuracy motion of robotic manipulators. The method is based on a smooth 7-phase sine jerk trajectory model, combined with a multi-joint MP trajectory velocity look-ahead strategy, enabling online generation of jerk-continuous and time-optimal MP synchronized motion trajectories. The characteristics of this method are summarized as follows:

(1) By equivalently transforming the complex 7-phase sine jerk model into the simple 3-phase trapezoidal velocity model, the computational complexity of trajectory planning is significantly reduced, enhancing real-time performance and providing essential support for robotic manipulators to generate motion trajectories online in real time.

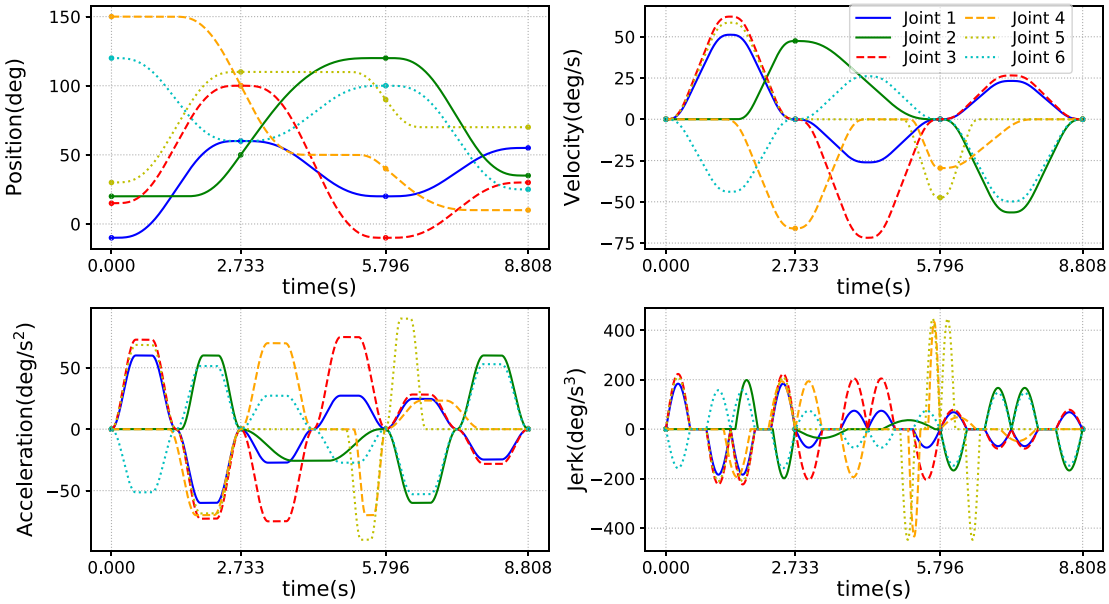


**Fig. 7.** Time-optimal multi-joint multi-point profiles resulted from the proposed method in task 4 ($\alpha = 0.75$).

**Table 8**
Execution times and tracking errors under various trajectory smoothing coefficients in task 5.

| Trajectory smoothing coefficient ($\alpha$) | Execution time (s) | Tracking error (deg) | | | | | |
|---|---|---|---|---|---|---|---|
| | | Joint 1 | Joint 2 | Joint 3 | Joint 4 | Joint 5 | Joint 6 |
| 0.1 | 7.144 | 2.89 | 3.18 | 4.06 | 3.74 | 3.31 | 2.83 |
| 0.5 | 8.041 | 2.58 | 2.83 | 3.61 | 3.33 | 2.95 | 2.51 |
| 0.75 | 8.808 | 2.35 | 2.59 | 3.30 | 3.04 | 2.69 | 2.29 |
| 1.0 | 9.848 | 2.11 | 2.31 | 2.95 | 2.72 | 2.41 | 2.05 |

**Fig. 8.** The manipulator utilized for the experiments in task 5.

(2) This method ensures the continuity of velocity, acceleration, and jerk throughout the entire trajectory without overshoot or undershoot, significantly enhancing the accuracy and smoothness of manipulator motion.
(3) By adjusting the trajectory smoothness coefficient, the balance between motion speed and trajectory smoothness can be reasonably regulated according to task requirements, enhancing the applicability of the method and enabling robots to better adapt to a variety of working scenarios and task demands.
(4) By calculating the peak jerk adaptively, a constant average trajectory acceleration is achieved, ensuring consistent acceleration capability of manipulators for paths of any length. Even in motion with dense path control points, the desired acceleration performance can be maintained.
(5) Based on the proposed multi-joint MP local velocity look-ahead strategy, this study achieves time-optimal MP trajectory planning for multi-joint manipulators. This strategy possesses the capability to adapt to any number of path control points and any number of joints, providing a flexible and efficient solution for motion planning of industrial robotic manipulators in complex and diverse tasks.

Although trajectory planning based on Cartesian space may be affected by singularity problems, tasks that require precise trajectory curves may still necessitate trajectory generation in Cartesian space. Therefore, future research will concentrate on extending the proposed method, with a particular focus on addressing relevant issues of time-optimal multi-joint MP trajectory planning in Cartesian space, aiming to further enhance the applicability and practicality of this approach.

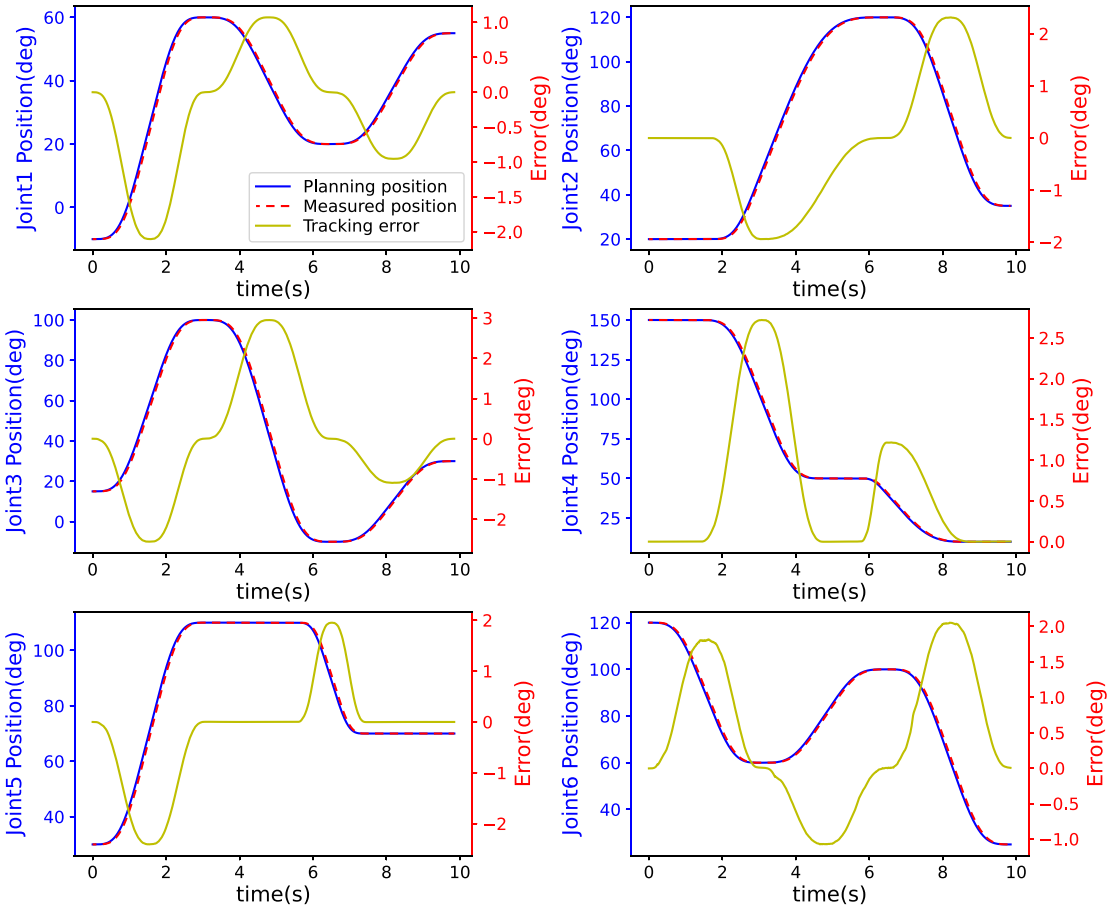


**Fig. 9.** Measured joint position profiles with tracking errors ($\alpha = 1.0$).

## CRediT authorship contribution statement

**Weiguang Yu:** Writing – original draft, Visualization, Validation, Software, Methodology, Investigation, Formal analysis, Data curation, Conceptualization. **Daokui Qu:** Writing – review & editing, Supervision, Investigation, Conceptualization. **Fang Xu:** Supervision, Project administration, Investigation. **Lei Zhang:** Supervision, Resources, Project administration, Investigation. **Fengshan Zou:** Supervision, Resources, Project administration, Funding acquisition. **Zhenjun Du:** Supervision, Resources, Funding acquisition.

## Declaration of competing interest

The authors declare that they have no known competing financial interests or personal relationships that could have appeared to influence the work reported in this paper.

## Acknowledgments

This work was supported in part by the National Key R&D Program of China (Grant No. 2019YFB1312201).

## References

Alpers, B. (2022). On fast jerk-continuous motion functions with higher-order kinematic restrictions for online trajectory generation. *Robotics*, *11*(4), 73. http://dx.doi.org/10.3390/robotics11040073.

Angeles, J. (2014). Fundamentals of robotic mechanical systems: theory, methods, and algorithms. In *Mechanical engineering series*: *vol. 124*, Cham: Springer International Publishing, http://dx.doi.org/10.1007/978-3-319-01851-5.

Bazaz, S. A., & Tondu, B. (1999). Minimum time on-line joint trajectory generator based on low order spline method for industrial manipulators. *Robotics and Autonomous Systems*, *29*(4), 257–268. http://dx.doi.org/10.1016/S0921-8890(99)00058-5.

Berscheid, L., & Kroeger, T. (2021). Jerk-limited real-time trajectory generation with arbitrary target states. In *Robotics: science and systems XVII*. Robotics: Science and Systems Foundation, http://dx.doi.org/10.15607/RSS.2021.XVII.015.

Biagiotti, L., & Melchiorri, C. (2008). *Trajectory planning for automatic machines and robots*. Berlin Heidelberg: Springer, http://dx.doi.org/10.1007/978-3-540-85629-0.

Biagiotti, L., Melchiorri, C., & Moriello, L. (2020). Damped harmonic smoother for trajectory planning and vibration suppression. *IEEE Transactions on Control Systems Technology*, *28*(2), 626–634. http://dx.doi.org/10.1109/TCST.2018.2882340.

Bobrow, J., Dubowsky, S., & Gibson, J. (1985). Time-optimal control of robotic manipulators along specified paths. *The International Journal of Robotics Research*, *4*(3), 3–17. http://dx.doi.org/10.1177/027836498500400301.

Chettibi, T. (2019). Smooth point-to-point trajectory planning for robot manipulators by using radial basis functions. *Robotica*, *37*(3), 539–559. http://dx.doi.org/10.1017/S0263574718001169.

Duque, D. A., Prieto, F. A., & Hoyos, J. G. (2019). Trajectory generation for robotic assembly operations using learning by demonstration. *Robotics and Computer-Integrated Manufacturing*, *57*, 292–302. http://dx.doi.org/10.1016/j.rcim.2018.12.007.

Fang, Y., Hu, J., Liu, W., Shao, Q., Qi, J., & Peng, Y. (2019). Smooth and time-optimal S-curve trajectory planning for automated robots and machines. *Mechanism and Machine Theory*, *137*, 127–153. http://dx.doi.org/10.1016/j.mechmachtheory.2019.03.019.

Fang, S., Ma, X., Zhao, Y., Zhang, Q., & Li, Y. (2019). Trajectory planning for seven-DOF robotic arm based on quintic polynormial. In *2019 11th international conference on intelligent human-machine systems and cybernetics* (pp. 198–201). Hangzhou, China: IEEE, http://dx.doi.org/10.1109/IHMSC.2019.10142.

Fang, Y., Qi, J., Hu, J., Wang, W., & Peng, Y. (2020). An approach for jerk-continuous trajectory generation of robotic manipulators with kinematical constraints. *Mechanism and Machine Theory*, *153*, Article 103957. http://dx.doi.org/10.1016/j.mechmachtheory.2020.103957.

Fung, R. F., & Cheng, Y. H. (2014). Trajectory planning based on minimum absolute input energy for an LCD glass-handling robot. *Applied Mathematical Modelling*, *38*(11–12), 2837–2847. http://dx.doi.org/10.1016/j.apm.2013.11.017.

Gasparetto, A., & Zanotto, V. (2007). A new method for smooth trajectory planning of robot manipulators. *Mechanism and Machine Theory*, *42*(4), 455–471. http://dx.doi.org/10.1016/j.mechmachtheory.2006.04.002.

Gasparetto, A., & Zanotto, V. (2010). Optimal trajectory planning for industrial robots. *Advances in Engineering Software*, *41*(4), 548–556. http://dx.doi.org/10.1016/j.advengsoft.2009.11.001.

Heo, H. J., Son, Y., & Kim, J. M. (2019). A trapezoidal velocity profile generator for position control using a feedback strategy. *Energies*, *12*(7), 1222. http://dx.doi.org/10.3390/en12071222.

Hu, J., Xiao, L., Wang, Y., & Wu, Z. (2006). An optimal feedrate model and solution algorithm for a high-speed machine of small line blocks with look-ahead. *International Journal of Advanced Manufacturing Technology*, *28*(9–10), 930–935. http://dx.doi.org/10.1007/s00170-004-1884-2.

Huang, J., Hu, P., Wu, K., & Zeng, M. (2018). Optimal time-jerk trajectory planning for industrial robots. *Mechanism and Machine Theory*, *121*, 530–544. http://dx.doi.org/10.1016/j.mechmachtheory.2017.11.006.

Lee, A. C., Lin, M. T., Pan, Y. R., & Lin, W. Y. (2011). The feedrate scheduling of NURBS interpolator for CNC machine tools. *Computer-Aided Design*, *43*(6), 612–628. http://dx.doi.org/10.1016/j.cad.2011.02.014.

Li, H., Wu, W. J., Rastegar, J., & Guo, A. (2019). A real-time and look-ahead interpolation algorithm with axial jerk-smooth transition scheme for computer numerical control machining of micro-line segments. *Proceedings of the Institution of Mechanical Engineers, Part B (Management and Engineering Manufacture)*, *233*(9), 2007–2019. http://dx.doi.org/10.1177/0954405418809768.

Lin, C., Chang, P., & Luh, J. (1983). Formulation and optimization of cubic polynomial joint trajectories for industrial robots. *IEEE Transactions on Automatic Control*, *28*(12), 1066–1074. http://dx.doi.org/10.1109/TAC.1983.1103181.

Moghaddam, M., & Nof, S. Y. (2016). Parallelism of pick-and-place operations by multi-gripper robotic arms. *Robotics and Computer-Integrated Manufacturing*, *42*, 135–146. http://dx.doi.org/10.1016/j.rcim.2016.06.004.

Nguyen, K. D., Ng, T. C., & Chen, I. M. (2008). On algorithms for planning S-curve motion profiles. *International Journal of Advanced Robotic Systems*, *5*(1), 11. http://dx.doi.org/10.5772/5652.

Pham, H., & Pham, Q. C. (2018). A new approach to time-optimal path parameterization based on reachability analysis. *IEEE Transactions on Robotics*, *34*(3), 645–659. http://dx.doi.org/10.1109/TRO.2018.2819195.

Piazzi, A., & Visioli, A. (2000). Global minimum-jerk trajectory planning of robot manipulators. *IEEE Transactions on Industrial Electronics*, *47*(1), 140–149. http://dx.doi.org/10.1109/41.824136.

Siciliano, B., Sciavicco, L., Villani, L., & Oriolo, G. (2009). Robotics. In *Advanced textbooks in control and signal processing*, London: Springer, http://dx.doi.org/10.1007/978-1-84628-642-1.

Simon, D., & Isik, C. (1993). A trigonometric trajectory generator for robotic arms. *International Journal of Control*, *57*(3), 505–517. http://dx.doi.org/10.1080/00207179308934404.

Su, T., Cheng, L., Wang, Y., Liang, X., Zheng, J., & Zhang, H. (2018). Time-optimal trajectory planning for delta robot based on quintic pythagorean-hodograph curves. *IEEE Access*, *6*, 28530–28539. http://dx.doi.org/10.1109/ACCESS.2018.2831663.

Trigatti, G., Boscariol, P., Scalera, L., Pillan, D., & Gasparetto, A. (2018). A new path-constrained trajectory planning strategy for spray painting robots - rev.1. *International Journal of Advanced Manufacturing Technology*, *98*(9–12), 2287–2296. http://dx.doi.org/10.1007/s00170-018-2382-2.

Tsai, M. S., Nien, H. W., & Yau, H. T. (2010). Development of a real-time look-ahead interpolation methodology with spline-fitting technique for high-speed machining. *International Journal of Advanced Manufacturing Technology*, *47*(5–8), 621–638. http://dx.doi.org/10.1007/s00170-009-2220-7.

Valente, A., Baraldo, S., & Carpanzano, E. (2017). Smooth trajectory generation for industrial robots performing high precision assembly processes. *CIRP Annals*, *66*(1), 17–20. http://dx.doi.org/10.1016/j.cirp.2017.04.105.

Visioli, A. (2000). Trajectory planning of robot manipulators by using algebraic and trigonometric splines. *Robotica*, *18*(6), 611–631. http://dx.doi.org/10.1017/S0263574700002721.

Wang, H., Wang, H., Huang, J., Zhao, B., & Quan, L. (2019). Smooth point-to-point trajectory planning for industrial robots with kinematical constraints based on high-order polynomial curve. *Mechanism and Machine Theory*, *139*, 284–293. http://dx.doi.org/10.1016/j.mechmachtheory.2019.05.002.

Wang, J. B., & Yau, H. T. (2009). Real-time NURBS interpolator: Application to short linear segments. *International Journal of Advanced Manufacturing Technology*, *41*(11–12), 1169–1185. http://dx.doi.org/10.1007/s00170-008-1564-8.

Wu, Z., Chen, J., Zhang, D., Wang, J., Zhang, L., & Xu, F. (2023). A novel multi-point trajectory generator for robotic manipulators based on piecewise motion profile and series-parallel analytical strategy. *Mechanism and Machine Theory*, *181*, Article 105201. http://dx.doi.org/10.1016/j.mechmachtheory.2022.105201.

Xie, Z., Wu, P., & Ren, P. (2016). A comparative study on the pick-and-place trajectories for a delta robot. In *Volume 5A: 40th mechanisms and robotics conference*. Charlotte, North Carolina, USA: American Society of Mechanical Engineers, http://dx.doi.org/10.1115/detc2016-59359, V05AT07A040.

Ye, P., Shi, C., Yang, K., & Lv, Q. (2008). Interpolation of continuous micro line segment trajectories based on look-ahead algorithm in high-speed machining. *International Journal of Advanced Manufacturing Technology*, *37*(9–10), 881–897. http://dx.doi.org/10.1007/s00170-007-1041-9.